

**Activity # 03 - Granite Cutting Tools**

- Granite is well-known for being a very dense, hard, and durable rock.
- It's this durability plus its natural aesthetics that makes it popular in homes and offices.
- It's also pricey, ranging from \$15 to \$40 per square foot.
- Professional installation adds to the cost with \$25-\$35 per square foot.

**Types of Granite Cutting Tools**

**Diamond Masonry Blades:**



- In order to properly cut through granite, you are going to need the right type of blade.
- Granite is a very tough type of material, and you won't be able to make a dent in it with normal blades.
- You need to have diamond blades in order to cut granite properly.
- One of the most typical types of diamond blades that are used to cut granite is the diamond masonry blade.
- This blade can be attached to many different types of saws.
- It will be capable of making precise cuts to granite.
- The blade being shown here features fourteen teeth that are segmented.

**Diamond Contour Blades:**



- Curved cutting is going to be possible with this blade
- People use these types of blades when they are installing granite countertops or sinks.
- Granite is a very common and popular material in bathrooms and kitchens.

### Diamond Circular Saw Blades:



- This blade will actually be really useful for cutting ceramic, porcelain and even marble.
- Granite jobs will always be a lot easier when you have this blade, and you will be able to rely on it for a long time.
- It is built to be a durable blade, so you won't have to change the blade out as often as you would some of the others.
- You are meant to use this blade on a tile saw that is being used for wet cuts.
- It isn't recommended for dry cutting.

### Diamond Profile Wheels:



- These wheels can grind down and polish granite without any problems.
- You simply need to install the diamond profile wheels in something like a variable speed polisher in order to make use of them.
- Once everything is installed, you'll be able to get to work.
- You can polish the granite and make sure that it looks fantastic.
- If you are going to be installing granite countertops, then this is going to be an essential purchase.

### Diamond Grinding Cup Wheels:



- Diamond grind cup wheels are similar to the profile wheels mentioned above in many ways.
- The difference between them is that these are used more for smoothing out the granite and truly finishing the project.
- The profile wheels will be great for edging the granite and providing the shape.
- You can then switch to the grinding cup wheels to smooth out the surface and put on those finishing touches.

### Diamond Drill Bits:



- Diamond drill bits are important for when you need to drill holes in granite.
- They can be installed in your power drill with relative ease.
- You'll be able to drill the proper types of holes that you need, so long as you have the right drill bits.

### Miter Saw:



- These miter saws are pretty easy to move to a job site, so they can be very convenient overall.
- When installed with the proper diamond saw blade, you'll be able to make precise cuts into granite surfaces.
- It will be perfect for cutting tiles or other granite items.

**Variable Speed Polisher/Grinder:**



- You will be making use of this variable speed polisher and grinder in order to finish up granite countertops.
- This is a powerful tool that is actually quite simple to use.
- You will be able to feel very natural while holding this tool.
- This will work well for either wet stone polishing or dry stone polishing.
- The fact that it is versatile in this way makes the tool that much more appealing.

**Angle Grinder:**



- This is good for when you're installing countertops, sinks, and other types of granite products.
- The angle grinder being shown here is a truly useful tool.
- It comes with a diamond blade and grinding wheels.
- This makes it useful for the purpose of working with granite

**Power Drills:**



- There are also going to be times when you will need to drill into granite.
- It's going to be capable of drilling holes in granite so that you can complete your task.
- This will always be easy when you have a power drill that is simple to operate.

**Dust Mask:**



- This isn't a cutting tool, but it will be a good idea to purchase a dust mask to wear during your job.
- You don't want to breathe in the dust that you are kicking up while cutting into the granite.
- Buying a simple and affordable dust mask can prevent you from having problems, so purchase one before starting out just to be safe.



## Open Archive Toulouse Archive Ouverte (OATAO)

OATAO is an open access repository that collects the work of Toulouse researchers and makes it freely available over the web where possible.

This is an author-deposited version published in: <http://oatao.univ-toulouse.fr/>  
Eprints ID: 11918

**Identification Number:** DOI:10.1007/s00170-014-6120-0

Official URL: <http://dx.doi.org/10.1007/s00170-014-6120-0>

### To cite this version:

Seguy, Sébastien and Arnaud, Lionel and Insperger, Tamás *Chatter in interrupted turning with geometrical defects: an industrial case study*. (2014) The International Journal of Advanced Manufacturing Technology, vol. 75 (n° 1-4). pp. 45-56. ISSN 0268-3768

# Chatter in interrupted turning with geometrical defects: an industrial case study

Sébastien Seguy · Lionel Arnaud · Tamás Insperger

**Abstract** In this paper, machine tool chatter arising in an interrupted turning process is investigated in a strong industrial context with a complex flexible part. A detailed analysis of the real cutting process is performed with special respect to the geometrical defects of the part in order to highlight the source of machine tool vibrations. The analysis is completed by simple models to estimate the forced vibrations in interrupted turning, the gyroscopic effect, and the mode coupling using a new simplified formulation. Then, a new dynamical model with interrupted cutting and geometrical inaccuracies—runout and orientation of eccentricity—is presented. Stability analysis of this model is performed by the semi-discretization method, an improved technique for analyzing delay-differential equations. The use of all these models on a given machining configuration allows comparing several vibration mechanisms. Thus, behavior's specificities are highlighted, especially the influence of eccentricity runout on stability. A sensitivity analysis shows the effect of the value and the orientation of the geometrical defects for low speed conditions. Then this result are extrapolated to high-speed conditions to look for possible new stable cutting conditions and shows a period doubling flip instability, never described

before in turning operations. The main focus of this paper is developing and exploring a stability model for interrupted cutting in turning with geometrical defects. The complexity of the industrial context led to methodically compare different chatter and vibration mechanisms; this approach can be generalized to other industrial contexts.

**Keywords** Interrupted turning · Chatter · Stability · Semi-discretization · Geometrical defects · Industrial context

## 1 Introduction

The productivity of machining operations is often limited by vibrations. Especially, the self-excited vibration—or chatter—degrades the surface finish of the part, increases the tool wear and reduces the spindle lifespan. However, this phenomenon is not new, already in 1907 F.W. Taylor wrote, “Chatter is the most obscure and delicate of all the problem facing the machinist, and in the case of castings and forgings of miscellaneous shapes probably no rules or formula can be devised which will accurately guide the machinist in taking the maximum cuts and speeds possible without producing chatter” [1]. The chatter is generally induced by the time delay between two consecutive part revolutions. By the effect of some small external disturbance, the tool starts a damped oscillation relative to the workpiece and the surface roughness is undulated. For the next revolution—in turning—the chip thickness is modulated. The equations of motion modeling such mechanism are typically delay-differential equations (DDE). This regenerative mechanism is well known and presented first for turning process [2, 3]. Since these works, many researchers have improved the knowledge by the well-known stability lobe representation and its adaptation to special cases [4–8].

Several complementary methods to simulate chatter exist in the literature. The most powerful, potentially, are numerical

---

S. Seguy (✉)  
Université de Toulouse, INSA, ICA (Institut Clément Ader), 135 Avenue de Rangueil, 31077 Toulouse Cedex 4, France  
e-mail: sebastien.seguy@insa-toulouse.fr

L. Arnaud  
Université de Toulouse, École Nationale d'Ingénieurs de Tarbes (ENIT), Laboratoire Génie de Production (LGP), 47 Avenue d'Azereix, BP 1629, 65016 Tarbes Cedex, France  
e-mail: lionel.arnaud@enit.fr

T. Insperger  
Department of Applied Mechanics, Budapest University of Technology and Economics, 1521 Budapest, Hungary  
e-mail: insperger@mm.bme.hu

methods using time-domain simulation of the equation of motion. These methods may simulate phenomenon at the scale of the cutting tooth, or even at the scale of the tip of the tool, for surface roughness prediction [9]. Methods using finite elements to model the tool-part contact are promising but remain limited by the complexity of the mechanical models and by the long-time simulation for realistic machining operations. Currently, they still do not provide the expected comprehensive approach [10] and simplified model must be used. Thus, since the early 2000s, various approaches based on the analysis of the stability of models using DDE have been presented [11, 12]. These approaches are powerful for the detection of classical Hopf instability, and they can also detect period doubling (also called flip) instability. This last instability is typical for highly interrupted cutting, like for milling with small radial engagement [13]. In particular, the semi-discretization method developed and improved by Insperger and Stépán seems to be a reliable and a powerful technique [14–16] and has been successfully applied to the analysis of different cutting processes [17–21].

The stability of turning process was often modeled by systems to 1 degree-of-freedom (DOF), 2 DOF, or 3 DOF mass-spring dampers. With this modeling, analytical predictions have been developed for orthogonal cutting to plot stability diagrams [22, 23]. Minis et al. [24] used the Nyquist criterion as an alternative approach to obtain the chatter-free conditions. However, this approach can be applied only to 1 DOF models. Two DOF models were developed for the case where the workpiece and the tool are flexible [25]. Chandiramani and Pothala [26] presented a 2 DOF model of the cutting tool, which involves the nonlinearity when the tool leaves the cut due to large chatter amplitudes. Control of chatter in case of a 1 DOF model was analyzed in [27]. The turning process is also analyzed by the nonlinear dynamics of a state-dependent delay model, in order to mitigate the chatter by nonlinear energy sink [28]. A numerical continuation technique is developed, which can be used to follow the periodic orbits of a system with implicitly defined state-dependent delays [29]. Dombovari et al. [30] presented a model of orthogonal cutting to analyze large amplitude motions. The model was formulated as a DDE and included the regenerative effect and the nonlinearity when contact between the cutting tool and the workpiece is lost.

Models have been developed for stability analysis of some special cases of boring process in [31, 32]. These classical approaches use a 1 or 2 DOF model and derive the classical stability lobe for perfect process, i.e., without geometrical defect and without interrupted cutting. Budak and Ozlu [33] extended the model to a multi-DOF system. The effects of the three cutting angles, the insert nose radius, and the dynamics of the components were included in the cutting system in all directions in a 3 DOF model. The case of interrupted turning was presented theoretically in the work of Szalai and Stépán

[34]. Like for milling operations, the highly interrupted turning leads to a period doubling instability for certain parameter combinations. In practice, there are several geometrical defects, which influence the dynamics and sometimes destroy the simple structure of the stability lobes. One of them is the eccentricity where the geometric axis of the turning part differs from the rotation axis. However, this defect was only analyzed for milling process stability [35] and 1-period (or cyclic fold) bifurcation arises including runout [36]. To the best knowledge of the authors [37], relatively little work has been published on interrupted turning and nothing for turning with flexible workpiece including geometrical defects.

This article focuses on the stability analysis of interrupted turning with geometrical defects where the workpiece is flexible. Various vibration mechanisms are investigated to explain the experimental results: forced vibrations related to interrupted cutting forces, regenerative vibrations related to surface undulation and delay, mode coupling vibrations between two orthogonal eigenmodes, and gyroscopic effect for high spindle speed [37]. A new dynamical model is developed to describe the effect of the eccentricity of the workpiece, as the runout effect was clear during experiments. Theoretical stability predictions are obtained using the semi-discretization method. The article is organized as follows. The industrial context and cutting test analysis are presented in Sect. 2. The model of interrupted turning with geometrical defects is described in Sect. 3. Simulation results are discussed in Sect. 4. Finally, the study is concluded in Sect. 5.

## 2 Experimental approach

This section presents the experimental approach developed with all the specifications, constraints of mass production and the results obtain in this context. First, the industrial context of experimental analysis is presented, then the modal analysis is conducted, then the geometrical inaccuracies—runout—are analyzed, and finally the stability is investigated with frequency analysis.

### 2.1 Industrial context

The *Ford Aquitaine Industries* factory manufactures automatic transmissions for the US market. Automatic transmissions are composed of the following parts: input shaft (connected to the motor), the inverter (clutch), various planetary gearboxes with clutches and brakes associated with different gear ratios, the oil pump (which supplies the pressure for controlling the clutches and brakes), the hydraulic control valve, and finally, the output shaft, which transmits motion to the wheels. The current study deals with the vibrations during the machining of a ring element, which supports a shaft passing through the oil pump. This ring element is made of bronze and serves as a

guide, but it must also allow oil circulation through its angular sectors (Fig. 1). The manufacturing process is fully automated. The assemblage generates geometrical defects between the support and the ring; therefore, the diameter of mounting on the lathe and the diameter of the ring are not exactly concentric. These defects—the value and the orientation of eccentricity—are slightly different for different assemblies due to manufacturing tolerances. The support of the pump is not a body of revolution because of the gear pump. In order to machine the various surfaces, a special mandrel is used to shift the rotation center and to keep equilibrated the system during machining (Fig. 2). The adjustable eccentricity of the mandrel may generate flexibly, increase the overhang part, and generate runout on the machine.

In this real industrial problem, all the constraints of mass production are imposed, i.e., limited time for on-site experiments and unavoidable on-site measurement inaccuracies.

## 2.2 Modal analysis

Before machining, hammer impact tests are made on the following items: ring hollow shaft support, workpiece, tool, and spindle. Since the tool is found to be rigid compared with the other elements, its stiffness and frequency response is neglected in the study. The corresponding frequency-response functions (FRF) of the workpiece is obtained by a hammer impact tests using an instrumented hammer (2302-10, Endevco), a velocimeter (VH300+, Ometron), and a data-acquisition system (Pulse, Brüel & Kjær). It became clear that the hollow shaft is by far the most flexible element; this result is also confirmed by a simplified finite element calculations. Figure 2 shows the setup of the frequency-response measurement. For the hollow shaft, two very close frequencies are found at approximately 1,800 Hz along the  $x$ -axis and 1,850 Hz along the  $y$ -axis, with a stiffness of 15 N/ $\mu\text{m}$  and a damping ratio of 0.7 %. Since the system is not axisymmetric, the difference between the FRF in different radial directions (e.g., in the  $x$  and  $y$  directions) can clearly be explained. The modal parameters are collected in Table 1. Finite element analysis of a simplified geometry of the pump support assembly with the hollow shaft and the ring provided a frequency very close to the one obtained by impulse test with accuracy less than 10 Hz. In fact, a simple cantilever beam model also provides the same frequency with accuracy around 50 Hz.

## 2.3 Geometrical defects analysis

Each assembly contains three machined parts. Every day, 10 assemblies out of 1,200 are scraped due to their nonconformability; moreover, the need for visual inspection of all the workpieces also increases the

manufacturing costs. The complexity of the manufacturing process is also an important aspect. Each of the three workpieces of the assembly is produced through two or three groups of machining operations, each of them involving three or four machine tools resulting in about 50 different combinations for each workpiece, and thus  $50 \times 50 \times 50$  possible combinations for the assembled products. Thus, systematic analyses of the defects in each operation step on each assembly are practically impossible. An identification of the numerous factors that are the possible sources of the vibration has been developed [38].

In this study, it is shown that there is no simple correlation between geometrical defects, at various stage of the process, and the vibrations observed. The main geometrical defects are the concentricity and the perpendicularity (Fig. 3), but the combination of these defects does not explain systematically the onset of vibrations.

Moreover, a very detailed study of the manufacturing process over several weeks has shown that operators were able to make some subtle adjustments, improving slightly the quality of the production. Unfortunately it is not possible to determine exact procedures because these adjustments are done below the graduated scales on the machines. For example, such subtle adjustments on tool height and concentricity of the workpiece holder may reduce the scrap ratio below 1 % for a while, but unfortunately it was almost impossible to reduce the average scrap ratio to less than 1 %.

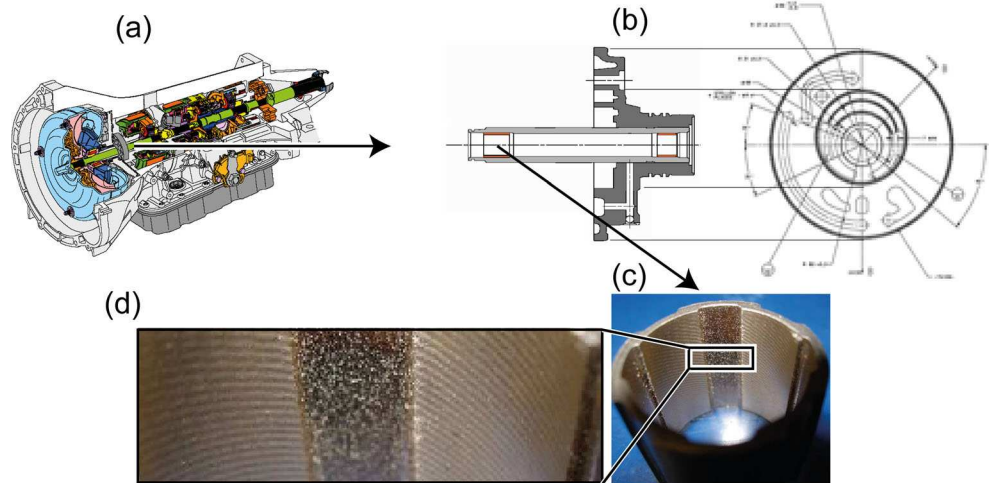
Comparison with other similar machining processes in the factory, not subjected to vibrations, has shown that stiffness of the workpiece-tool-machine system is probably also an important factor, but again it does not explain the occurrence of the vibrations alone.

Finally, because this machining process is at very high level of production, it is not realistic to consider major modifications of the process to reduce the vibration, because the cost associated would be too high. Practically, results from a preliminary study show that a small adjustment on the cutting angle resulted in a major improvement of the scrap ratio even if the real source of the problem has not been clearly identified at this stage [38]. The aim of this paper is to try to go further in the analysis of the phenomenon.

## 2.4 Stability problem and frequency analysis

The spindle speed is 2,200 rpm ( $V_c=131$  m/min); radial engagement during semifinishing is 0.12 mm and during finishing is 0.05 mm. At the beginning, the process was designed for a single-step finishing with 0.17 mm radial pass, but because of vibrations it has never been possible and semifinishing has been introduced. The lead angle of the tool is  $\kappa=95^\circ$ , the axial and the radial cutting angles are  $\gamma_1=\gamma_2=$

**Fig. 1** Sectional view of the transmission (a), support of the pump (b), ring workpiece (c), and detail about machined surface (d)



$-8^\circ$ , respectively, and the nose radius is  $r=0.8$  mm; a diamond insert PC<sub>50</sub> is used with no lubrication (dry machining).

The optical analysis of the vibrations on the machined surface allows approximating the associated frequencies (Fig. 4). By measuring the number of vibration marks on one of the four sectors and by extrapolation over the nonmachined sectors, one can count around 50 marks per revolution. Considering that the workpiece spindle speed is 2,200 rpm, these marks correspond to a frequency of 1,833 Hz. The helix associated to these marks is due to the fact that the number of vibration cycles per workpiece revolution is not an integer, thus a phase shift appear during machining and create the helix. Some workpieces showed rapid variations of this helix angle; this demonstrates that dynamic behavior may vary quickly along the machining.

Acoustic measurement during machining showed the same main frequency, around 1,850 Hz, illustrated in Fig. 5. During machining, the frequency slightly increases but only around 0.2 %. The same vibration frequency was measured by a laser velocimeter at the rotating workpiece and by a piezoelectric accelerometer on the spindle.

### 3 Model of interrupted turning with geometrical defects

This section presents the modeling approach developed in order to explain and reduce the vibrations during interrupted turning with geometrical defects. First, the forced vibrations in interrupted turning are estimated by a simple model, then a simple gyroscopic model is presented, after the mode coupling is studied, and finally a new dynamic modeling for interrupted turning is presented.

#### 3.1 Forced vibrations in interrupted turning

First, forced vibrations in interrupted turning are investigated in order to explain the vibration problem. With the cutting parameters and according to the tool manufacturer, the tangential and the radial force components are respectively about 30 N and about 5 N. During the initial development process, cutting forces were estimated at 150 and 20 N. Due to the presence of too-frequent vibrations, the finishing was divided into two steps (Sect. 2.4). It may be noted that a force of 10 N corresponds to a static bending of about 0.7  $\mu\text{m}$ , which is the

**Fig. 2** Frequency-response measurement



**Table 1** Modal parameters identified

$m$	$\xi$	$k$	$\omega_0$
0.1135 kg	0.7 %	$15 \times 10^6$ N/m	11498.4 rad/s

same order as the amplitude of the machining grooves (of the order of 1  $\mu\text{m}$ ).

In interrupted turning, the cutting forces are not constant. In order to show the various harmonics of the main cutting force,

$$F(t) = 0.62F_0 \left[ 1 + 0.95\cos\left(\frac{2\pi t}{T}\right) - 0.35\cos\left(\frac{4\pi t}{T}\right) - 0.14\cos\left(\frac{6\pi t}{T}\right) + 0.26\cos\left(\frac{8\pi t}{T}\right) - 0.06\cos\left(\frac{10\pi t}{T}\right) - 0.13\cos\left(\frac{12\pi t}{T}\right) + 0.13\cos\left(\frac{14\pi t}{T}\right) + 0.02\cos\left(\frac{16\pi t}{T}\right) - 0.11\cos\left(\frac{18\pi t}{T}\right) + 0.06\cos\left(\frac{20\pi t}{T}\right) \right], \quad (1)$$

where  $F_0$  is the mean value of the cutting force.

Compared with experiments, no harmonic of the shock passing frequency (2,200 rpm with four sectors of cut) of 146.6 Hz is present from 1,800 to 1,850 Hz (nearest harmonics are no. 12 ( $a_{12}$ ) and no. 13 ( $a_{13}$ ) at 1,760 and 1,906 Hz, respectively). In addition, the coefficients are very low for both closest harmonics (respectively -0.08 and 0.01). Considering the maximum resonance, the forced displacement  $d_{\max}$  is expressed as follow:

$$d_{\max} = \frac{a_{12}F}{k2\xi}, \quad (2)$$

with a 10 N radial force, the forced displacement would be 3.8  $\mu\text{m}$ . Although resonance effect has the capability to

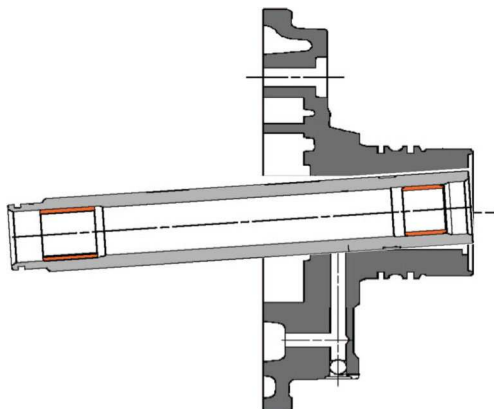


**Fig. 3** Geometrical defects of the workpiece

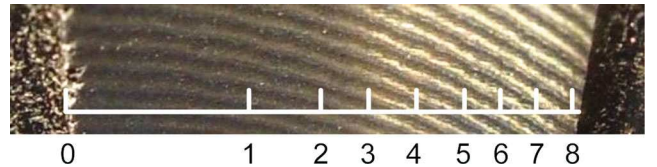


**Fig. 4** Visual analysis of the part by micrography

the Fourier expansion of a typical interrupted cutting force is considered as an illustration. Only the first ten harmonics (Fig. 6) are kept, and the following expression was found:

generate the observed defects, we will investigate other vibration mechanisms. First, we will naturally investigate gyroscopic effect to try to explain a possible frequency shift that would lead to resonance.

### 3.2 Gyroscopic effect

As mentioned in Sect. 2.2, the system can be modeled by a simple rotating flexible beam of length  $L$  as shown in Fig. 7.

The equation of motion for a rotating beam can be classically expressed as follow, including the gyroscopic effects:

$$\begin{bmatrix} m & 0 \\ 0 & m \end{bmatrix} \begin{Bmatrix} \ddot{q}_1 \\ \ddot{q}_2 \end{Bmatrix} + \Omega \begin{bmatrix} 0 & -a \\ a & 0 \end{bmatrix} \begin{Bmatrix} \dot{q}_1 \\ \dot{q}_2 \end{Bmatrix} + \begin{bmatrix} k & 0 \\ 0 & k \end{bmatrix} \begin{Bmatrix} q_1 \\ q_2 \end{Bmatrix} = \begin{Bmatrix} 0 \\ 0 \end{Bmatrix}, \quad (3)$$

where  $\Omega$  is spindle speed and  $q_i$  is the modal displacement in the  $i$  directions, i.e., transverse to the axis of the cantilever. The mass  $m$  is defined by

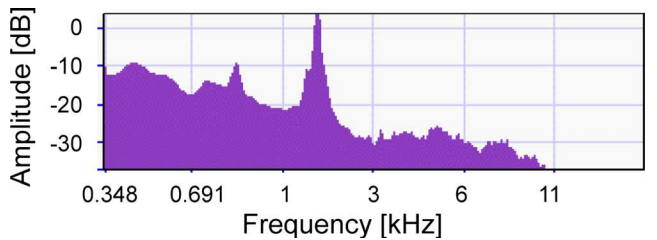


**Fig. 5** Audio spectral

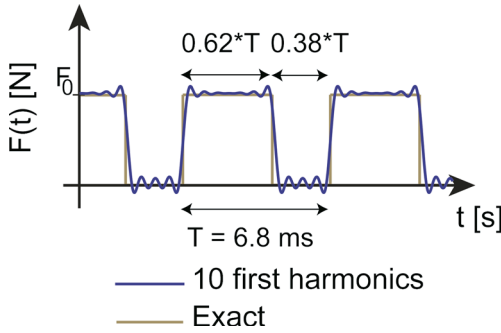


Fig. 6 Approximate cutting force

$$m = \int_0^L \frac{1}{2} \rho S \Phi^2(x) dx, \quad (4)$$

where  $\rho$  is the density,  $S$  is the section of the beam, and  $\Phi(x)$  is the modal shape.

The stiffness  $k$  reads

$$k = \int_0^L \frac{1}{2} EI \ddot{\Phi}^2(x) dx, \quad (5)$$

where  $E$  is the modulus of elasticity and  $I$  is the moment of inertia. The coefficient  $a$  is

$$a = \int_0^L 2\rho I \dot{\Phi}(x) \Phi(x) dx. \quad (6)$$

The function  $\Phi$  is classically approximated using the modal shape of first mode of the nonrotating beam.

The classical analytical treatment of the Eq. (3) gives the following two vibration frequencies:

$$\omega_1 = \sqrt{\omega_0^2 + \frac{a^2 \Omega^2}{2m^2} \left( 1 - \sqrt{1 + \frac{4m^2 \omega_0^2}{a^2 \Omega^2}} \right)}, \quad (7)$$

Fig. 7 Simplified gyroscopic model

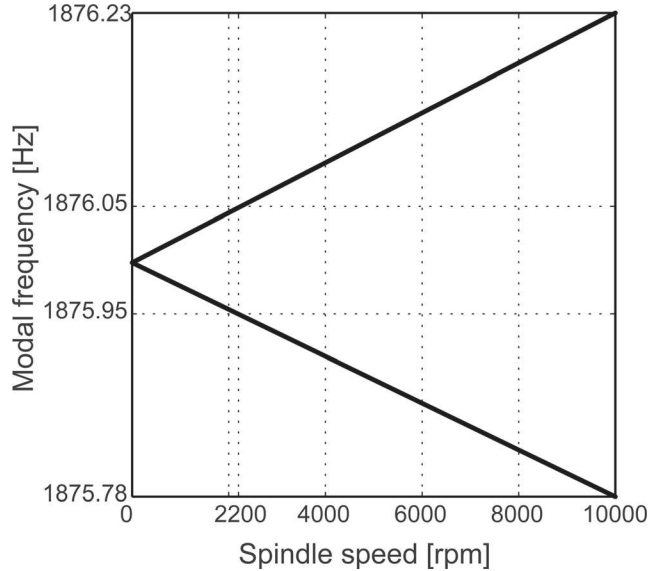
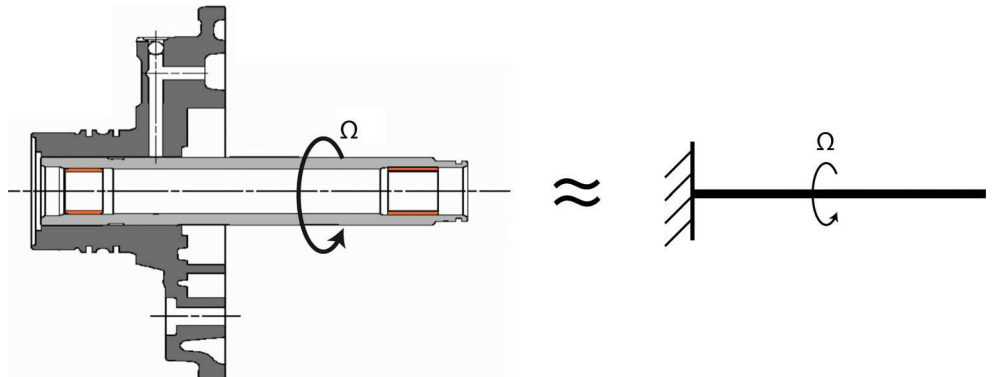


Fig. 8 Campbell diagram

$$\omega_2 = \sqrt{\omega_0^2 + \frac{a^2 \Omega^2}{2m^2} \left( 1 + \sqrt{1 + \frac{4m^2 \omega_0^2}{a^2 \Omega^2}} \right)}. \quad (8)$$

The corresponding Campbell diagram can be seen in Fig. 8. As it can be seen, the separation of the dual mode of bending in two modes, by gyroscopic effect is negligible, less than  $\pm 0.0125\%$  at 10,000 rpm.

As a conclusion, the gyroscopic effect cannot explain a sufficient shift in frequency to lead to resonance. We will then now study the mode coupling effect, well known as primary chatter, to try to explain the phenomenon observed.

### 3.3 Mode coupling effect: primary chatter

The first explanation of the phenomenon of the mode coupling effect was given by Tlusty et al. [3]. Because exact calculation is quite complex, we may approximate the magnitude of the phenomenon. Let us suppose that the movement of the

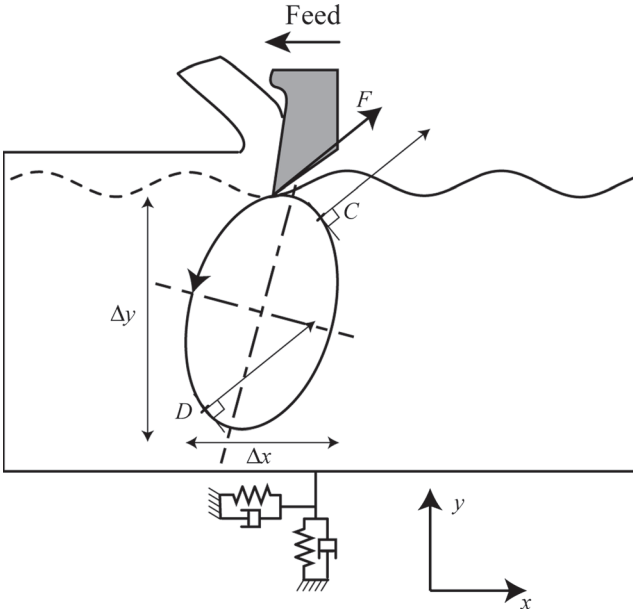


**Fig. 9** Movement during mode coupling

flexible part is elliptical, as described in Fig. 9. During the C to D path, energy is dissipated because the movement is against the cutting force. Then during the D to C path, energy is gained and more than what dissipated because the cutting force is greater. At the same time, some energy is always dissipated by the damping of the system. Thus, vibrations are the result of equilibrium between damping loss and cutting force energy provided during oscillations.

The damping force energy  $W_1$  during one cycle is approximated by:

$$W_1 \approx c \times V \times L, \quad (9)$$

with  $c$  the damping,  $V$  the average velocity, and  $L$  the path length of the displacement.

The length of the ellipse is approximated by  $\pi(\Delta x + \Delta y)$ , and if we consider that the modes are quite orthogonal and with similar amplitudes, the expression of  $W_1$  is approximated by:

$$W_1 \approx 2m\xi\omega_0 \frac{\pi(\Delta x + \Delta y)}{2\pi} \pi(\Delta x + \Delta y). \quad (10)$$

The cutting force energy  $W_2$  during one cycle is expressed by:

$$W_2 = \oint_{\text{ellipse}} F_x dx + F_y dy, \quad (11)$$

with,

$$x = \Delta x \cos \theta; y = \Delta y \sin \theta; dx = -\Delta x \sin \theta d\theta; dy = \Delta y \cos \theta d\theta. \quad (12)$$

If we consider a linear cutting law:

$$F_x = -A_p K_t (y_0 + y); F_y = -A_p K_r (y_0 + y). \quad (13)$$

Substituting (12)–(13) in Eq. (11),  $W_2$  is expressed by:

$$W_2 = \int_0^{2\pi} -A_p K_t (y_0 + \Delta y \sin \theta) (-\Delta x \sin \theta) d\theta + \int_0^{2\pi} -A_p K_r (y_0 + \Delta y \sin \theta) \Delta x \cos \theta d\theta. \quad (14)$$

If we consider that  $F_y$  component has a null energy during one cycle and that  $F_x$  component is linear with  $x$ ,  $W_2$  is approximated by

$$W_2 \approx A_p K_t \Delta x \Delta y \pi. \quad (15)$$

With  $A_p$  the length of the cutting edge engaged (along  $z$  axis) and  $K_t$  the tangential cutting force coefficient (i.e., in  $x$  direction).

The equilibrium condition of energy, is

$$W_1 = W_2. \quad (16)$$

Assuming that  $\Delta x \approx \Delta y$ , which is a large simplification of course but  $\Delta x$  and  $\Delta y$  must anyway be in the same order of magnitude for the coupling effect to take place, so it comes:

$$2m\xi\omega_0 \frac{2\pi\Delta x}{2\pi} \approx A_p K_t \Delta x \Delta y \pi. \quad (17)$$

The maximal depth of cut without primary chatter is then:

$$A_p \approx \frac{4m\xi\omega_0^2}{K_t}, \quad (18)$$

with the parameters collected in Tables 1 and 2, the limit depth of cut is  $\approx 1.5$  mm. This approximation shows that in our context, primary chatter could probably not appear. Moreover, according to [3], the modes coupling may occur only when the orientation of the lower frequency mode is between the cutting force and the normal of the machined surface. In our context, with a near axisymmetric system, the modes are near  $x$ - and  $y$ -axes and the radial cutting force is toward the workpiece; it is, thus, quite impossible to reach this condition thus to have primary chatter.

### 3.4 Mechanical model

The mechanical model of the turning process is shown in Fig. 10. A preliminary study showed that the gyroscopic effect is negligible (Sect. 3.2), therefore, the part can be described by a 1 DOF system (Table 1, Sect. 2.2), in the  $x$  direction.

The dynamic model is defined by the following equation:

$$m\ddot{x}(t) + c\dot{x}(t) + kx(t) = F_x(t), \quad (19)$$

**Table 2** Cutting parameters

$t_{ci}$	$t_{fi}$	$K_t$
0.156	0.094	270 MPa

where  $m$  is the modal mass,  $c$  is the damping,  $k$  is the stiffness, and  $F_x(t)$  is the cutting force. The cutting force is expressed by a linear cutting law:

$$F_x(t) = A_p(t)K_t g(t)(x(t)-x(t-\tau)), \quad (20)$$

where  $A_p(t)$  is the depth of cut, which is time dependent due to the runout,  $K_t$  is the tangential cutting coefficient and  $\tau$  is the regenerative time delay:

$$\tau = \frac{60}{\Omega}, \quad (21)$$

where  $\Omega$  is the spindle speed in rpm. Function  $g(t)$  is a  $T$ -periodic screen function, it is equal to 1 if the tool is cutting, and 0 if the tool is vibrating freely:

$$g(t) = \begin{cases} 1 & \text{if } \text{mod}(t, T) \leq T_{ci} \\ 0 & \text{if } \text{mod}(t, T) \leq T_{ci} + T_{fi} \\ 1 & \text{if } \text{mod}(t, T) \leq T_{ci} + T_{fi} + T_{c2} \\ \vdots & \\ 0 & \text{if } T - T_{fi} < \text{mod}(t, T) \leq T \end{cases}, \quad (22)$$

where  $\text{mod}(t, T)$  denotes the modulo function (e.g.,  $\text{mod}(12, 5)=2$ ),  $T_{ci}$  and  $T_{fi}$ ,  $i=1, 2, \dots, n$  are the periods of cutting and free motions associated to the angular sectors shown in Fig. 10, and  $T=\sum_{i=1}^n(T_{ci}+T_{fi})$  is the rotation period of the workpiece. The scaled values  $t_{ci}$  and  $t_{fi}$  are summarized in Table 2. Note that  $T$  is the rotation period, which is equal to the regenerative delay  $\tau$ .

The eccentricity is described by two parameters:  $d$  is the absolute value of the runout and  $\alpha$  is the orientation angle of the runout compared with the onset of the machined segments.

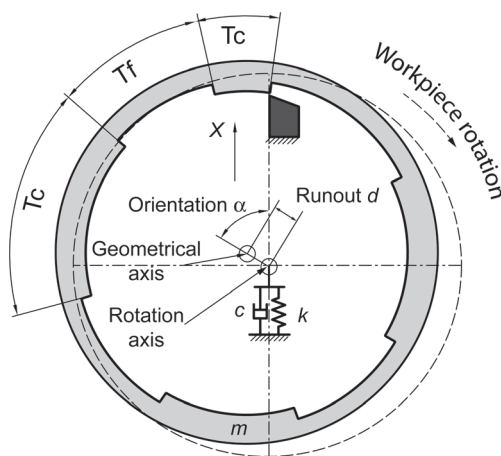


**Fig. 10** Mechanical model of the interrupted turning process with geometrical defects

The actual time-dependent depth of cut can be expressed as:

$$A_p(t) = A_{p,id} - d \cos\left(\frac{\Omega 2\pi}{60}t - \alpha\right), \quad (23)$$

where  $A_{p,id}$  is the axial depth of cut in the ideal case without any eccentricity.

This new mechanical model contains all the parameter for analysis of stability in interrupted turning process with geometrical inaccuracies, i.e., runout and orientation of eccentricity.

#### 4 Theoretical stability predictions

This section presents the theoretical predictions. First, the semi-discretization method is presented and the specifications are highlighted. Then the stability study is conducted in the case of real industrial case, and finally the results are extrapolated to the high-speed domain to highlight the appearance of flip lobes, in turning, which is new.

##### 4.1 Semi-discretization method

The semi-discretization method is presented according to [15], it is a well-known method, validated in many configurations machining [16]. Equations (19) and (20) imply:

$$\dot{\mathbf{x}}(t) = \mathbf{A}(t)\mathbf{x}(t) + \mathbf{B}(t)u(t-\tau), \quad (24)$$

$$u(t) = \mathbf{C}\mathbf{x}(t), \quad (25)$$

with

$$\mathbf{x}(t) = \begin{pmatrix} x(t) \\ \dot{x}(t) \end{pmatrix}, \quad \mathbf{A}(t) = \begin{pmatrix} 0 & 1 \\ \frac{A_p(t)K_t g(t)}{m} - \omega_0^2 & -2\zeta\omega_0 \end{pmatrix},$$

$$\mathbf{B}(t) = \begin{pmatrix} 0 \\ \frac{A_p(t)K_t g(t)}{m} \end{pmatrix}, \quad \mathbf{C} = (1 \ 0),$$

where  $\omega_0^2=k/m$  is the dominant angular natural frequency of the workpiece and  $\zeta=c/(2m\omega_0)$  is the damping ratio. Equations (24) and (25) form a DDE with periodic coefficients. Note that the period of the system is equal to the regenerative delay, i.e.,  $\mathbf{A}(t)=\mathbf{A}(t+\tau)$  and  $\mathbf{B}(t)=\mathbf{B}(t+\tau)$ . The stability is analyzed by the first-order semi-discretization method [15, 16]. The approximate semidiscrete system for Eq. (24) reads

$$\dot{\mathbf{y}}(t) = \mathbf{A}_j \mathbf{y}(t) + \mathbf{B}_j (\beta_1(t)v(t_{j-r+1}) + \beta_0(t)v(t_{j-r})), \quad t \in [t_j, t_{j+1}], \quad (26)$$

$$v(t) = \mathbf{C}\mathbf{y}(t), \quad (27)$$

where  $t_j=j\Delta t$ ,  $\Delta t=\tau/n$  is the discretization step,  $n$  is an integer approximation parameter and

$$\mathbf{A}_j = \frac{1}{\Delta t} \int_{t_j}^{t_{j+1}} \mathbf{A}(t) dt, \quad \mathbf{B}_j = \frac{1}{\Delta t} \int_{t_j}^{t_{j+1}} \mathbf{B}(t) dt,$$

$$\beta_1(t) = \frac{t-\tau-(j-n)\Delta t}{\Delta t}, \quad \beta_0(t) = \frac{t-\tau-(j-n+1)\Delta t}{\Delta t}.$$

The system (26)–(27) can be solved as an ODE over the discretization interval  $[t_j, t_{j+1}]$  resulting in the discrete map

$$y(t_{j+1}) = P_j y(t_j) + R_{j,0} v(t_{j-r}) + R_{j,1} v(t_{j-r+1}), \quad (28)$$

where

$$\mathbf{P}_j = e^{\mathbf{A}_j \Delta t},$$

$$\mathbf{R}_{j,0} = - \int_0^{\Delta t s - \tau + (n-1)\Delta t} \frac{1}{\Delta t} e^{\mathbf{A}_j (\Delta t - s)} \mathbf{B}_j ds,$$

$$\mathbf{R}_{j,1} = \int_0^{\Delta t s - \tau + n\Delta t} \frac{1}{\Delta t} e^{\mathbf{A}_j (\Delta t - s)} \mathbf{B}_j ds.$$

If  $\mathbf{A}_j$  is a regular matrix then the above integration gives

$$\mathbf{R}_{j,0} = \left( \mathbf{A}_j^{-1} + \frac{1}{\Delta t} \left( \mathbf{A}_j^{-2} - (\tau - (r-1)\Delta t) \mathbf{A}_j^{-1} \right) (\mathbf{I} - e^{\mathbf{A}_j \Delta t}) \right) \mathbf{B}_j,$$

$$\mathbf{R}_{j,1} = \left( \mathbf{A}_j^{-1} + \frac{1}{\Delta t} \left( -\mathbf{A}_j^{-2} - (\tau - r\Delta t) \mathbf{A}_j^{-1} \right) (\mathbf{I} - e^{\mathbf{A}_j \Delta t}) \right) \mathbf{B}_j.$$

Using state-augmentation, the discrete time system can be written as an

$$\mathbf{z}(t_{j+1}) = \mathbf{G}_j \mathbf{z}(t_j), \quad (29)$$

with  $\mathbf{z}(t_j) = \text{col}(\mathbf{y}(t_j) \quad v(t_{j-1}) \quad v(t_{j-2}) \quad \dots \quad v(t_{j-n}))$  and

$$\mathbf{G}_j = \begin{pmatrix} \mathbf{P}_j & \mathbf{0} & \cdots & 0 & \mathbf{R}_{j,1} & \mathbf{R}_{j,0} \\ \mathbf{C} & 0 & \cdots & 0 & 0 & 0 \\ 0 & 1 & \cdots & 0 & 0 & 0 \\ \vdots & \vdots & \ddots & \vdots & \vdots & \vdots \\ 0 & 0 & \cdots & 1 & 0 & 0 \end{pmatrix}, \quad (30)$$

Multiple repeated applications of Eq. (30) with initial state  $\mathbf{z}(t_0)$  gives the Floquet transition matrix for the semidiscrete system (26)–(27) in the form  $\Phi = \mathbf{G}_j \mathbf{G}_{j-1} \dots \mathbf{G}_0$ . Actually,  $\Phi$  provides a finite dimensional approximation of the infinite-dimensional monodromy operator of the original system (19)–(20).

The stability of the approximate system (26)–(27) can be assessed by the eigenvalue analysis of matrix  $\Phi$ . If all the eigenvalues are inside the unit circle of the complex plane, then the system (24)–(25) is asymptotically stable. Since semi-discretization preserves asymptotic stability of the original system (19)–(20), the method can be used to construct approximate stability charts.

## 4.2 Stability analysis in industrial context

Stability charts are determined for interrupted turning without geometrical defects with the dynamic and cutting coefficient from Tables 1 and 2. The approximation parameter for the semi-discretization method is  $r=300$ . This parameter was selected in order to have good approximation for lower spindle speeds. The stability lobes—made with a  $200 \times 150$  grid resolution of the parameter plane—are shown in Fig. 11. The unstable, chatter domains are denoted by gray shading.

In this industrial context, the spindle speed of the lathe is limited to 2,300 rpm, which is associated with the 50th Hopf lobe. It is not typical in the literature to encounter regenerative spindle speeds around the 50th Hopf lobe [37]. At these spindle speeds, there are about 20 rpm difference between a maximum and a minimum stable depth of cut, which corresponds to less than 1 % of the spindle speed. The vertical position of the optimal area is shifted proportionally to the modal frequency, which may vary from about 0.5 % of a workpiece to another.

The impacts of geometrical defects (eccentricity and orientation) are now studied through 3D graph representations, on the area of the 50th Hopf lobe. Three characteristic spindle speeds are investigated (Fig. 11):

- 2,230 rpm corresponding to the minimal depth of cut (point A),
- 2,250 rpm corresponding to a medium depth of cut (point B),
- 2,259 rpm corresponding to the maximal depth of cut (point C).

For each case, the critical depths of cut were determined for several eccentricity and orientation using the semi-discretization method.

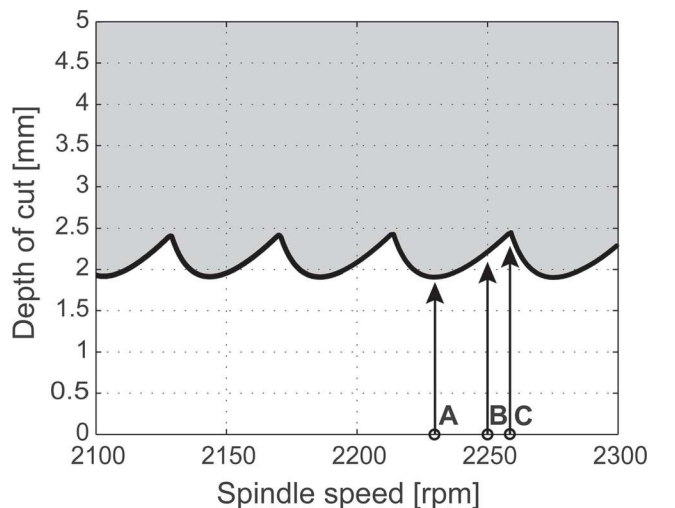


**Fig. 11** Classical stability lobes for the industrial context, without geometrical defect

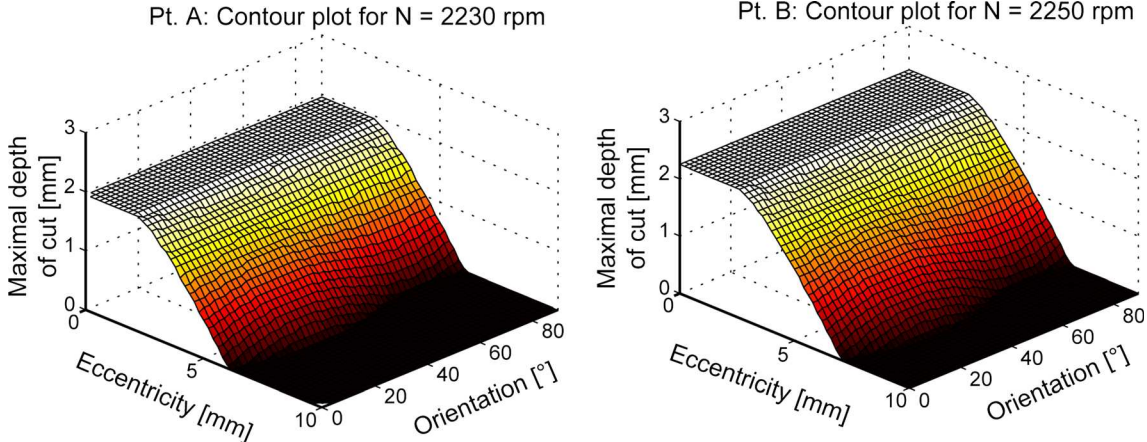


**Fig. 12** Map of stability, influence of the geometrical defects (eccentricity and orientation) on the maximal chatter free depth of cut. *Left*, 2,230 rpm (Pt. A). *Right*, 2,250 rpm (Pt. B)

The results for a spindle speed of 2,230 and 2,250 rpm are presented in Fig. 12 in 3D plot form. The diagram was constructed by computing the maximal depth of cut, without chatter, over a  $50 \times 46$ -sized grid of eccentricity and orientation parameters. Without geometric defect, the critical depth of cut is maximal. The effect of the orientation defect is negligible, because the critical depth of cut is always the same for various orientations between  $0^\circ$  and  $90^\circ$ . On the other hand, the value of the eccentricity has an important impact on the process stability. Three areas are present on the contour plot (Fig. 12). For small defects, up to 3 mm, the process stability is not affected. For a defect between 3 and 6 mm, the critical depth of cut decreases quite linearly. If the defect is higher than 6 mm, then it's impossible to machine the part without chatter.

Finally, Fig. 13 presents also a similar contour plot for a spindle speed of 2,259 rpm. The limiting value of the eccentricity is increased to 8 mm, just because of the spindle speed chosen.

On the area of the 50th lobe, based on the above numerical

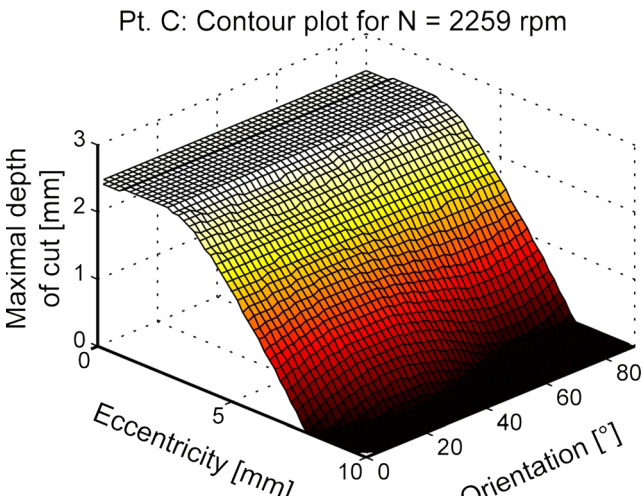


**Fig. 13** Map of stability at 2,259 rpm (Pt. C)

studies, it can be concluded that the most critical parameter is the value of the eccentricity, and the dependence on the defect orientation is negligible.

The results show that regenerative effect cannot explain the observed phenomenon, which showed the occurrence of chatter even for a few micrometers of eccentricity. However, since the effect of the geometrical defects has been quite rarely studied in interrupted cutting, the authors investigated the spindle speed range at around the first and the second stability lobes, even if experimental data were out of reach, because it is worth investigating the flip lobes, never described before in turning,

#### 4.3 Extrapolation of the stability properties to the high-speed domain

In this section, the effect of geometrical defects is investigated on the area of the first Hopf lobe, corresponding to high-speed machining cutting conditions. In this case, the separation of the dual mode of bending in two modes, by gyroscopic effect is negligible, less than  $\pm 0.36\%$  at 300,000 rpm. The stability lobes are plotted for various eccentricity and two defects orientation for extremely large spindle speeds Fig. 14.

Similarly to low-spindle speed machining, the influence of the defect orientation on stability is negligible. As shown in Fig. 14, the stability lobes are the same for orientations of  $0^\circ$  and  $30^\circ$ . Complementary simulations have generalized this result for any orientation between  $0^\circ$  and  $90^\circ$ .

The important impact of the eccentricity is presented on Fig. 14, for 0, 2, 5, 10, and 15 mm values.

- First, the eccentricity reduces the lower limit of stability lobes. For example, for a speed of 150 krpm, with no eccentricity, the critical depth of cut is 2.5 mm, but with a defect of 5 mm, the critical depth of cut decreases

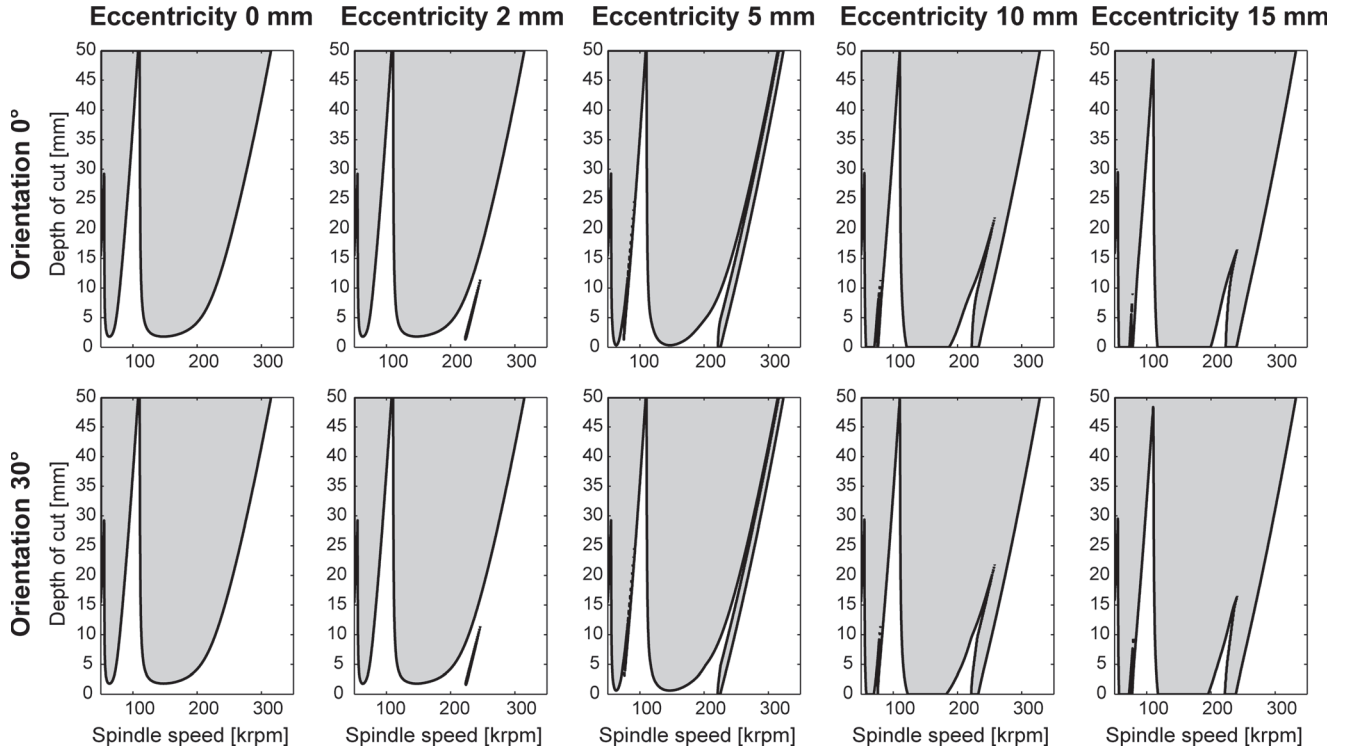


**Fig. 14** Stability lobes with geometrical defects (eccentricity and orientation) at high-speed machining, around the first lobe

practically to zero. Note that the tool is still cutting even if the nominal depth of cut is zero, since the actual depth of cut is not zero due to the relatively large eccentricity, which is commensurate to the depth of cut. Similarly to low speed machining, the defect of eccentricity has great impact on the process stability.

- Secondly, the eccentricity generates a special kind of instability next to the first Hopf lobe, similar to the well known flip lobe on interrupted milling [11]. This new instability is not generated by the interruption of the cutting, because without eccentricity the new unstable area is not shown on the stability lobe (Fig. 14). It is rather related to the eccentricity of the workpiece. At small eccentricity values, an unstable island are born very similarly as it was shown in [34]. Then, for larger eccentricities, the island opens up and forms a stability lobe similarly to the period doubling stability lobes of low radial immersion milling or interrupted turning.

A detailed analysis of the real cutting process is performed with special respect to the geometrical defects of the part in order to highlight the source of machine tool vibrations. Simplified models were developed for modeling the forced vibrations in interrupted turning, the gyroscopic effect and the mode coupling effect—primary chatter. These simplified formulations can be easily transposed in industrial applications because practically any of these vibration mechanisms may be the source of problems but complete investigations are usually out of reach in an industrial context.

A new stability modeling for interrupted turning is proposed. The model is based on the semi-discretization method, improved by the important aspect of interrupted cutting and geometrical inaccuracies (value and orientation of eccentricity). A sensitivity analysis of this model showed that the stability of the machining process is mainly sensitive to the value of the eccentricity, while the orientation of the defect from the interrupted cutting zones has no influence.

The extrapolation in high-speed machining, i.e., around the first stability lobe, show that a new zone of instability appears similarly to the flip lobes of low radial immersion milling or interrupted turning. This instability is only generated by the eccentricity and it is not related to the interruption of the cutting process. These flip lobes have never been reported before in turning.

This global approach with improved models (forced vibrations, gyroscopic effect, and primary chatter) and a new regenerative interrupted model including geometrical defects

## 5 Concluding remarks

In this work, the stability of interrupted turning process with geometrical defects is investigated in a practical perspective of mass production.

can be used to build a systematic approach for analyzing vibrations in other industrial contexts with geometrical defects. The authors emphasize the fact that in industrial contexts several vibration mechanisms are in competition and must be systematically compared, and that geometrical defects must be taken into consideration.

**Acknowledgments** The authors acknowledge the French Ministry of Science and the Hungarian National Science Foundation under grant OTKA-K105433 for their financial support. Ford Aquitaine Industries provided the research opportunity.

## References

- Taylor FW (1907) On the art of cutting metals. *Trans ASME* 28:31–350, §634A
- Tobias SA, Fishwick W (1958) Theory of regenerative machine tool chatter. *Engineer* 205(199–203):238–239
- Thlusty J, Polacek M (1963) The stability of the machine tool against self-excited vibration in machining. In: Proceedings of the International Research in Production Engineering Conference, ASME Press, Pittsburgh, pp. 465–474
- Altintas Y, Budak E (1995) Analytical prediction of stability lobes in milling. *CIRP Ann Manuf Technol* 44:357–362
- Budak E (2006) Analytical models for high performance milling, part I: cutting forces, structural deformations and tolerance integrity. *Int J Mach Tools Manuf* 46:1478–1488
- Budak E (2006) Analytical models for high performance milling, part II: process dynamics and stability. *Int J Mach Tools Manuf* 46:1489–1499
- Gourc E, Seguy S, Arnaud L (2011) Chatter milling modeling of active magnetic bearing spindle in high-speed domain. *Int J Mach Tools Manuf* 51:928–936
- Mousseigne M, Landon Y, Seguy S, Dessein G, Redonnet JM (2013) Predicting the dynamic behaviour of torus milling tools when climb milling using the stability lobes theory. *Int J Mach Tools Manuf* 65: 47–57
- Paris H, Peigné G, Mayer R (2004) Surface shape prediction in high speed milling. *Int J Mach Tools Manuf* 44:1567–1576
- Lorong P, Coffignal G, Cohen-Assouline S (2008) Simulation du comportement dynamique d'un système usinant: modélisation de l'interaction outil/matière en présence d'une pièce flexible. *Mec Ind* 9:117–124
- Insperger T, Mann BP, Stépán G, Bayly PV (2003) Stability of up-milling and down-milling, part 1: alternative analytical methods. *Int J Mach Tools Manuf* 43:25–34
- Bayly PV, Halley JE, Mann BP, Davies MA (2003) Stability of interrupted cutting by temporal finite element analysis. *J Manuf Sci Eng* 125:220–225
- Khasawneh FA, Bobrenkov OA, Mann BP, Butcher EA (2012) Investigation of period-doubling islands in milling with simultaneously engaged helical flutes. *J Vib Acoust* 134:021008
- Insperger T, Stépán G (2004) Updated semi-discretization method for periodic delay-differential equations with discrete delay. *Int J Numer Methods Eng* 61:117–141
- Insperger T, Stépán G, Turi J (2008) On the higher-order semi-discretizations for periodic delayed systems. *J Sound Vib* 313:334–341
- Insperger T, Stépán G (2011) Semi-discretization for time-delay systems—stability and engineering applications. Springer
- Mann BP, Insperger T, Stépán G, Bayly PV (2003) Stability of up-milling and down-milling, part 2: experimental verification. *Int J Mach Tools Manuf* 43:35–40
- Insperger T, Stépán G (2004) Stability analysis of turning with periodic spindle speed modulation via semidiscretization. *J Vib Control* 10:1835–1855
- Zatarain M, Muñoz J, Peigné G, Insperger T (2006) Analysis of the influence of mill helix angle on chatter stability. *CIRP Ann Manuf Technol* 55:365–368
- Seguy S, Insperger T, Arnaud L, Dessein G, Peigné G (2011) Suppression of period doubling chatter in high-speed milling by spindle speed variation. *Mach Sci Technol* 15:153–171
- Seguy S, Dessein G, Arnaud L, Insperger T (2010) Control of chatter by spindle speed variation in high-speed milling. *Adv Mater Res* 112: 179–186
- Altintas Y, Weck M (2004) Chatter stability of metal cutting and grinding. *CIRP Ann Manuf Technol* 53:619–642
- Olgac N, Sipahi R (2005) A unique methodology for chatter stability mapping in simultaneous machining. *J Manuf Sci Eng* 127:791–800
- Minis IE, Magrab EB, Pandelidis IO (1990) Improved methods for the prediction of chatter in turning part 3: a generalized linear theory. *J Eng Ind* 112:28–35
- Chen CK, Tsao YM (2006) Stability analysis of regenerative chatter in turning process without using tailstock. *Int J Adv Manuf Technol* 29:648–654
- Chandiramani NK, Pothala T (2006) Dynamics of 2-dof regenerative chatter during turning. *J Sound Vib* 290:448–464
- Lehotzky D, Insperger T (2012) Stability of turning processes subjected to digital PD control. *Period Polytech Mech Eng* 56: 33–42
- Gourc E, Seguy S, Michon G, Berlioz A (2013) Chatter control in turning process with a nonlinear energy sink. *Adv Mater Res* 698:89–98
- Insperger T, Barton DAW, Stépán G (2008) Criticality of Hopf bifurcation in state-dependent delay model of turning processes. *Int J Nonlinear Mech* 43:140–149
- Dombovari Z, Barton DAW, Wilson RE, Stepan G (2011) On the global dynamics of chatter in the orthogonal cutting model. *Int J Nonlinear Mech* 46:330–338
- Rigal J, Pupaza C, Bedrin C (1998) A model for simulation of vibrations during boring operations of complex surfaces. *CIRP Ann Manuf Technol* 47:51–54
- Lazoglu I, Atabay F, Altintas Y (2002) Dynamic of boring processes: part III—time domain. *Int J Mach Tools Manuf* 42:1567–1576
- Budak E, Ozlu E (2007) Analytical modeling of chatter stability in turning and boring operations: a multi-dimensional approach. *CIRP Ann Manuf Technol* 56:401–404
- Szalai R, Stépán G (2006) Lobes and lenses in the stability chart of interrupted turning. *J Comput Nonlinear Dyn* 1:205–211
- Schmitz TL, Couey J, Marsh E, Maunler N, Hughes D (2007) Runout effect in milling: surface finish, surface location error, and stability. *Int J Mach Tools Manuf* 47:841–851
- Insperger T, Mann BP, Surmann T, Stépán G (2008) On the chatter frequencies of milling processes with runout. *Int J Mach Tools Manuf* 48:1081–1089
- Siddhpura M, Paurobally R (2012) A review of chatter vibration research in turning. *Int J Mach Tools Manuf* 61:27–47
- Arnaud L, Dutilh V, Dessein G, Saussol A (2008) Arnaud M Analyse et réduction des vibrations d'usinage d'une pièce automobile produite en grande série. XVI Symposium VIbrations, SHocks & NOise VISHNO, Paris



International Conference On DESIGN AND MANUFACTURING, IConDM 2013  
**Influence of cutting parameters on cutting force and surface finish in turning operation**

Dr. C. J. Rao<sup>a\*</sup>, Dr. D. Nageswara Rao<sup>b</sup>, P. Srihari<sup>c</sup>

<sup>a</sup>Professor, Mechanical Engineering Dept., Aditya Institute of Technology and Management, Tekkali-532 201, Srikakulam (Dist.), Andhra Pradesh, India.

<sup>b</sup>Vice-Chancellor, CUTM, Parlakhemundi, Odisha, India

<sup>c</sup>Associate Professor, Mechanical Engineering Dept., Aditya Institute of Technology and Management, Tekkali-532 201, Srikakulam (Dist.), Andhra Pradesh, India.

---

### Abstract

This research reports the significance of influence of speed, feed and depth of cut on cutting force and surface roughness while working with tool made of ceramic with an  $\text{Al}_2\text{O}_3+\text{TiC}$  matrix (KY1615)and the work material of AISI 1050 steel (hardness of 484 HV). Experiments were conducted using Johnford TC35 Industrial type of CNC lathe. Taguchi method (L27 design with 3 levels and 3 factors) was used for the experiments. Analysis of variance with adjusted approach has been adopted. The results have indicated that it is feed rate which has significant influence both on cutting force as well as surface roughness. Depth of cut has a significant influence on cutting force, but has an insignificant influence on surface roughness. The interaction of feed and depth of cut and the interaction of all the three cutting parameters have significant influence on cutting force, whereas, none of the interaction effects are having significant influence on the surface roughness produced. If power consumption minimization is to be achieved for the best possible surface finish, the most recommended combination of feed rate and depth of cut is also determined.

© 2013 The Authors. Published by Elsevier Ltd. Open access under [CC BY-NC-ND license](#).

Selection and peer-review under responsibility of the organizing and review committee of IConDM 2013

**Keywords:** Full Factorial design; ANOVA; Surface roughness; Cutting force; Interaction Effect; Adjusted approach.

---

### 1. Introduction

Turning operation using a single point cutting tool has been one of the oldest and popular methods of metal cutting. It has even replaced grinding in several applications with reduced lead time without affecting the surface quality ([1], [2], [3], [4] and [5]). In this connection, two important aspects which are widely studied in turning operations are cutting forces and surface roughness of the work-piece. Process parameter optimization is of great significance while looking into the process capability of any machining operation. Shaw [6] has emphasized the importance of studying cutting forces in turning operations as a number of factors are influenced by it, namely, surface accuracy, tool wear, tool breakage, cutting temperature, self-excited and forced vibrations, etc. A group of researchers including Ozel and Karpat [7] have found that cutting parameters (Feed rate, Cutting Speed, Depth of Cut, tool geometry and material properties of tool) directly influence the surface finish of machined components. However, among the cutting force, thrust force, and feed force, the former prominently influences power consumption and this work considers only cutting force as one of the endogenous factors.

Surface roughness is also a vital measure as it may influence frictional resistance, fatigue strength or creep life of machined components. As far as turned components are concerned, better surface finish (low surface roughness) is important as it can reduce or even completely eliminate the need of further machining. Many researchers have found that

---

\* Corresponding author. Tel.: +919440416577; fax: +918945245266.  
E-mail address: [raoj\\_chintu@yahoo.com](mailto:raoj_chintu@yahoo.com)

surface roughness has bearing on heat transmission, ability to hold lubricant, surface friction, wearing etc. Despite the fact that surface roughness plays a very important role in the utility and life of a machined component due to its dependence on several process parameters and numerous uncontrollable factors machining process has no complete control over surface finish obtained. So, the venture of controlling process parameters so as to produce best surface finish is an on-going process varying from various material to tool combinations and the machining conditions. The present work is aimed at studying the influence of the three major process parameters in a turning operation, namely, speed, feed and depth of cut on cutting force and surface roughness for a predefined combination of material and tool under the given set of machining conditions.

Cutting force is basically the product of specific cutting energy coefficient ( $N/mm^2$ ), depth of cut (mm), and feed (mm/rev). Cutting force is generally resolved into three components, namely feed force ( $F_x$ ), thrust force ( $F_y$ ), and cutting force ( $F_z$ ). The thrust force has been the focus of study in many studies, as it is the most important among the three which has major bearing on parameters of research interest. The surface finish of any given part is measured in terms of average heights and depths of peaks and valleys on the surface of the work piece [6]. But there are basically two streams of arguments on the influencing factors of surface roughness. The first defines surface roughness as the ratio of  $f^2$  to  $32r$ , where  $f$  is the feed (mm/rev) and  $r$  is cutter nose radius (mm) ([6], [8], and [9]). According to the second equation surface roughness is a function of speed (mm/min) and feed (mm/rev) [10]. As such both cutting force and surface roughness is not an easy parameter to quantify as it depends on several process parameters including speed, feed, and depth of cut for different combinations of tool and work material.

## 2. Literature review

Literature is very rich in terms of turning operation owing to its importance in metal cutting. The three important process parameters in this research are speed, feed and depth of cut. Surface roughness of a turned work-piece is dependent on these process parameters and also on tool geometry: nose radius, rake angle, side cutting edge angle and cutting edge. In addition, it also depends on the several other exogenous factors such as: work piece and tool material combination and their mechanical properties, quality and type of the machine tool used, auxiliary tooling, and lubricant used, and vibrations between the work piece, machine tool and cutting tool ([6], [11], [12], [13], [14], [15], [16] and [7]).

Lin et al. [17] adopted an abductive network to construct a prediction model for surface roughness and cutting force. Feng and Wang [15] investigated the influence on surface roughness in finish turning operation by developing an empirical model through considering exogenous variables: work piece hardness (material), feed, cutting tool point angle, depth of cut, spindle speed, and cutting time. Suresh et al. [18] focused on machining mild steel by TiC-coated tungsten carbide (CNMG) cutting tools for developing a surface roughness prediction model by using Response Surface Methodology (RSM). Lee and Chen [19] have used ANN using sensing technique to monitor the effect of vibration produced by the motions of the cutting tool and work piece during the cutting process and developed an on-line surface recognition system. Kirby et al. [20] developed the prediction model for surface roughness in turning operation. Ozel and Karpat [7] worked on the prediction of surface roughness and tool flank wear by utilizing the neural network model in comparison with regression model. Kohli and Dixit [21] proposed a neural network based methodology with the acceleration of the radial vibration of the tool holder as feedback. Pal and Chakraborty [22] studied on development of a back propagation neural network model for prediction of surface roughness in turning operation and used mild steel work piece with HSS as the cutting tool for performing a large number of experiments. Sing and Lumar [23] studied on optimization of feed force through setting of optimal value of process parameters namely speed, feed and depth of cut in turning of EN24 steel with TiC coated tungsten carbide inserts. Ahmed [24] developed the methodology required for obtaining optimal process parameters for prediction of surface roughness in Al turning. Zhong et al. [25] predicted the surface roughness of turned surfaces using networks with seven inputs namely tool insert grade, work piece material, tool nose radius, rake angle, depth of cut, spindle speed, feed rate. Doniavi et al. [26] used RSM in order to develop empirical model for the prediction of surface roughness by deciding the optimum cutting condition in turning. Kassab and Khoshnaw [27] examined the correlation between surface roughness and cutting tool vibration for turning operation. Al-Ahmari [28] developed empirical models for tool life, surface roughness and cutting force for turning operation. Wang and Lan [29] used Orthogonal Array of Taguchi method coupled with grey relational analysis considering four parameters viz. speed, depth of cutting, feed rate, tool nose run off etc. for optimizing three responses: surface roughness, tool wear and material removal rate in precision turning on an ECOCA-3807 CNC Lathe. Sahoo et al. [30] studied for optimization of machining parameters combinations emphasizing on fractal characteristics of surface profile generated in CNC turning operation. Reddy et al. [31] adopted multiple regression model and ANN to deal with surface roughness prediction model for machining of aluminium alloys by CNC turning. Thamma [32] constructed the regression model to find out the optimal combination of process parameters in turning operation for Aluminium 6061 work piece. Fnides et al. [33] studied on machining of X38CrMoV5-1 steel treated at HRC by a mixed ceramic tool (insert CC650) to reveal the influence of cutting parameters: feed rate, cutting speed, depth of cut and flank

wear on cutting forces as well as on surface roughness. Zawada-Tomkiewicz [34] used multi-parameter characterization of the surface in turning operation on an EN41Cr4 low chromium alloy steel, heat treated to the hardness of 58 HRC using polycrystalline cubic boron nitride tools. Davis [35] attempted optimization of surface roughness in dry as well as wet turning operation of EN24 and found that none of the factors (speed, feed and depth of cut) was found to be significant.

The above literature review clearly indicates that the study of feed, speed and depth of cut on cutting force and surface roughness has been very active since the past several decades, but there has been a continuous need to extend this study for the different combinations of tool and work material. The literature review also shows that there is no much of work undertaken with mixed ceramic tool and AISI 1050 steel work material combination, despite the fact that it is a widely used combination owing to its industrial applications.

Hence, the main objective of this research is to study the significance of influence of speed, feed and depth of cut on cutting force on the tool and surface finish of the work piece. In addition, the work also makes an attempt to optimize the cutting parameters for minimum energy consumption while turning the given material using the specified tool.

### **3. Research methodology**

The research is basically a hypotheses testing research making use of design of experiments based on Taguchi method. Following hypotheses have been constituted for testing the main effect of the cutting parameters based on the literature review.

$H_{1a}$ : Speed has significant influence on cutting force in turning operation.

$H_{1o}$ : Speed has no significant influence on cutting force in turning operation.

$H_{2a}$ : Speed has significant influence on surface roughness of the work-piece in turning operation.

$H_{2o}$ : Speed has no significant influence on surface roughness of the work-piece in turning operation.

$H_{3a}$ : Feed rate has significant influence on cutting force in turning operation.

$H_{3o}$ : Feed rate has no significant influence on cutting force in turning operation.

$H_{4a}$ : Feed rate has significant influence on surface roughness of the work-piece in turning operation.

$H_{4o}$ : Feed rate has no significant influence on surface roughness of the work-piece in turning operation.

$H_{5a}$ : Depth of cut has significant influence on cutting force in turning operation.

$H_{5o}$ : Depth of cut has no significant influence on cutting force in turning operation.

$H_{6a}$ : Depth of cut has significant influence on surface roughness of the work-piece in turning operation.

$H_{6o}$ : Depth of cut has no significant influence on surface roughness of the work-piece in turning operation.

#### *3.1. Machine and the materials*

The turning operation was conducted using Johnford TC35 Industrial type of CNC lathe machine with a range of spindle speed from 50 rpm to 3500 rpm, and a 10 KW motor drive. The cutting tool was a mixed ceramic with an  $\text{Al}_2\text{O}_3+\text{TiC}$  matrix, which is designated by KY1615. The insert type was TNGA 160408-KY1615 and TNGA 160408-KY4400. The material used was a hardened AISI 1050 steel (hardness of 484 HV). These bars (40 mm in diameter and 300 mm in length) were machined under dry condition. The work material bars were trued, centred and cleaned by removing a 1 mm depth of cut from the outside surface, prior to the actual machining tests.

#### *3.2. Cutting force measurement*

The instrument used for the measurement of cutting force was IEICOS Multi-Component Force Indicator. It comprises of three independent digital display calibrated to display force directly using three component tool dynamometer. This instrument comprises independent DC excitation supply for feeding strain gauge bridges, signal processing systems to process and compute respective force values for direct independent display. Instrument operates on 230V, 50Hz AC mains. To record the force readings, IEICOS Multi-Component Force Indicator software was used. The data was obtained through a USB cable connected to the Dynamometer and stored on a computer.

#### *3.3. Surface roughness measurement*

The instrument used to measure surface roughness was Surtronics 3+. For a probe movement of 4mm, surface roughness readings were recorded at three locations on the work piece and the average value was used for analysis.

Specifications of Surtronics 3+:

- Gauge Range:  $\pm 150\text{um}$

- Probe Movement (max): 25.4mm
- Traverse speed: 1mm/s

### 3.4. Cutting conditions and experimental procedure

Among the speed, feed rate, and depth of cut combinations available on the Lathe, three levels of cutting parameters were selected based on similar earlier studies (Table – 1).

Table - 1: Factors and their Levels

Factor	Level 1	Level 2	Level 3
A: Speed (m/min)	50	75	95
B: Feed (mm/rev)	0.05	0.10	0.15
C: Depth of Cut (mm)	0.25	0.50	0.75

Taguchi design L-27 for three levels and three factors ( $3^k$ ) yielded 27 experiments and two replicates were carried out. The standard order, run order, cutting parameters and responses in the design of experiments are given table - 2.

Table 2: Design matrix with responses (cutting force and surface roughness)

Standard Order	Run Order	Speed (m/min) A	Feed (mm/rev) B	DOC (mm) C	Ra (μm)	Fy (kgf)	AB	BC	AC	ABC
39	1	75	0.05	0.75	5.95	23.00	39.60	0.08	270.00	29.70
5	2	50	0.10	0.50	7.34	17.00	41.04	0.09	114.00	20.52
45	3	75	0.15	0.75	7.49	33.00	90.00	0.19	270.00	67.50
26	4	95	0.15	0.50	8.73	27.00	112.50	0.13	225.00	56.25
36	5	50	0.15	0.75	6.75	25.00	57.00	0.19	171.00	42.75
3	6	50	0.05	0.75	4.45	20.00	25.08	0.08	171.00	18.81
19	7	95	0.05	0.25	5.61	15.00	49.50	0.03	112.50	12.38
27	8	95	0.15	0.75	9.67	30.00	112.50	0.19	337.50	84.38
53	9	95	0.15	0.50	8.20	23.00	112.50	0.13	225.00	56.25
52	10	95	0.15	0.25	8.53	22.00	112.50	0.06	112.50	28.13
23	11	95	0.10	0.50	7.01	14.00	81.00	0.09	225.00	40.50
44	12	75	0.15	0.50	10.20	23.00	90.00	0.13	180.00	45.00
31	13	50	0.10	0.25	7.86	12.00	41.04	0.05	57.00	10.26
8	14	50	0.15	0.50	10.00	23.00	57.00	0.13	114.00	28.50
20	15	95	0.05	0.50	6.01	18.00	49.50	0.06	225.00	24.75
49	16	95	0.10	0.25	7.77	12.00	81.00	0.05	112.50	20.25
7	17	50	0.15	0.25	9.60	15.00	57.00	0.06	57.00	14.25
38	18	75	0.05	0.50	5.66	16.00	39.60	0.06	180.00	19.80
47	19	95	0.05	0.50	8.66	18.00	49.50	0.06	225.00	24.75
14	20	75	0.10	0.50	6.32	13.00	64.80	0.09	180.00	32.40
22	21	95	0.10	0.25	6.91	12.00	81.00	0.05	112.50	20.25
2	22	50	0.05	0.50	3.96	15.00	25.08	0.06	114.00	12.54
21	23	95	0.05	0.75	7.36	20.00	49.50	0.08	337.50	37.13
41	24	75	0.10	0.50	8.53	14.00	64.80	0.09	180.00	32.40
33	25	50	0.10	0.75	8.35	22.00	41.04	0.14	171.00	30.78
16	26	75	0.15	0.25	10.60	19.00	90.00	0.06	90.00	22.50
25	27	95	0.15	0.25	9.21	15.00	112.50	0.06	112.50	28.13
12	28	75	0.05	0.75	7.93	21.00	39.60	0.08	270.00	29.70

10	29	75	0.05	0.25	4.02	12.00	39.60	0.03	90.00	9.90
42	30	75	0.10	0.75	8.06	24.00	64.80	0.14	270.00	48.60
40	31	75	0.10	0.25	5.25	12.00	64.80	0.05	90.00	16.20
54	32	95	0.15	0.75	11.07	26.00	112.50	0.19	337.50	84.38
28	33	50	0.05	0.25	4.28	10.00	25.08	0.03	57.00	6.27
6	34	50	0.10	0.75	6.53	23.00	41.04	0.14	171.00	30.78
9	35	50	0.15	0.75	8.93	25.00	57.00	0.19	171.00	42.75
43	36	75	0.15	0.25	10.93	16.00	90.00	0.06	90.00	22.50
32	37	50	0.10	0.50	8.90	19.00	41.04	0.09	114.00	20.52
30	38	50	0.05	0.75	4.92	25.00	25.08	0.08	171.00	18.81
1	39	50	0.05	0.25	4.20	8.00	25.08	0.03	57.00	6.27
13	40	75	0.10	0.25	7.60	12.00	64.80	0.05	90.00	16.20
48	41	95	0.05	0.75	7.86	20.00	49.50	0.08	337.50	37.13
17	42	75	0.15	0.50	9.53	26.00	90.00	0.13	180.00	45.00
4	43	50	0.10	0.25	9.20	12.00	41.04	0.05	57.00	10.26
18	44	75	0.15	0.75	9.80	27.00	90.00	0.19	270.00	67.50
51	45	95	0.10	0.75	6.93	17.00	81.00	0.14	337.50	60.75
15	46	75	0.10	0.75	9.00	26.00	64.80	0.14	270.00	48.60
34	47	50	0.15	0.25	9.61	16.00	57.00	0.06	57.00	14.25
24	48	95	0.10	0.75	7.59	20.00	81.00	0.14	337.50	60.75
50	49	95	0.10	0.50	6.26	12.00	81.00	0.09	225.00	40.50
46	50	95	0.05	0.25	6.66	6.00	49.50	0.03	112.50	12.38
37	51	75	0.05	0.25	6.73	14.00	39.60	0.03	90.00	9.90
29	52	50	0.05	0.50	5.65	15.00	25.08	0.06	114.00	12.54
35	53	50	0.15	0.50	10.01	26.00	57.00	0.13	114.00	28.50
11	54	75	0.05	0.50	6.86	15.00	39.60	0.06	180.00	19.80

#### 4. Result analysis

##### 4.1. Cutting force analysis

The analysis of variance (ANOVA) results very clearly support the hypotheses  $H_3$  &  $H_5$ , indicating that both feed and depth of cut have significant influence on cutting force (table 3). This is in agreement with earlier research undertaken by a group

Table - 3: ANOVA of Cutting Force.

Source	DF	Seq SS	Adj SS	Adj MS	F	P	Hypothesis
Speed	2	20.48	20.28	10.24	2.91	0.072	--
Feed	2	625.82	625.82	312.91	88.93	0.000*	Supported
DOC	2	1046.37	1046.37	523.19	148.69	0.000*	Supported
Speed*Feed	4	36.41	36.41	9.10	2.59	0.059	--
Speed*DOC	4	28.52	28.52	7.13	2.03	0.119	--
Feed*DOC	4	50.52	50.52	12.63	3.59	0.018*	Supported
Speed*Feed*DOC	8	85.26	85.26	10.65	3.01	0.015*	Supported
Error	27	95.00	95.00	3.52	--	--	
Total	53	1988.37	--	--	--	--	
<b>S = 1.88      R-Sq = 95.22%      R-Sq(adj) = 90.62%</b>							

\*Significant influence ( $\alpha = 0.05$ )

of researchers which was undertaken with different tool and material combination ([5], [36]). This can be seen in the main effect plot of cutting force (figure 1). Further, it can be observed that the interaction effect of feed rate & depth of cut and the interaction of all the three cutting parameters have significant influence on cutting force (table 3; figure 2). The R-square and adjusted R-square values above 90%, indicates that the model fit is on the higher side of the acceptable limit (figure 3). The regression coefficients of cutting force are given in table 4. The regression equation for cutting force is as follows. However, it can be observed that in the regression equation, it is only the depth of cut which has significant influence. Again, the R-square and R-square adjusted are both above 75%, and hence, the model is moderately a good fit. The regression equation is as follows.

$$F_y (\text{kgf}) = 4.35 - 0.107 * \text{speed} + 29.8 * \text{feed} + 25.8 * \text{depth of cut} + 0.129 * \text{speed} - 9.1 * \text{feed} * \text{depth of cut} - 0.043 * \text{speed} * \text{feed} * \text{depth of cut} + \epsilon$$

Where,  $\epsilon$  = regression error

Table - 4: Regression Analysis Cutting Force.

Predictor	Coef	SE Coef	T	P
Constant	4.35	5.12	0.85	0.40
Speed	-0.11	0.07	-1.51	0.14
Feed	29.81	52.66	0.57	0.57
DOC	25.84	6.5	4.00	0.000
Speed*Feed	0.13	0.09	1.36	0.18
Feed*DOC	-9.06	52.08	-0.17	0.86
Speed*Feed*DOC	-0.04	0.11	-0.38	0.71
<b>S = 2.93      R-Sq = 79.7%      R-Sq(adj) = 77.1%</b>				

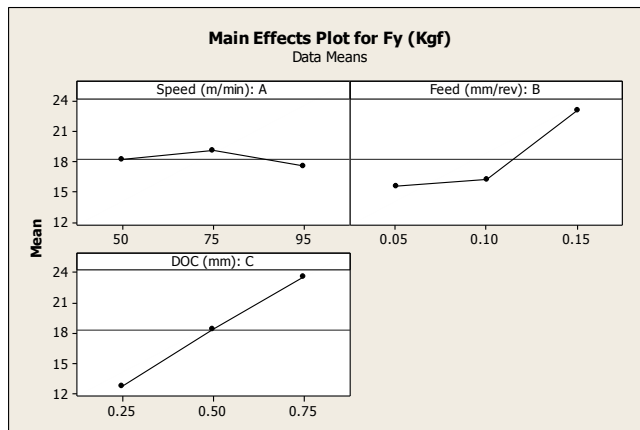


Figure - 1: Main Effects Plot for Cutting Force  $F_y$ .

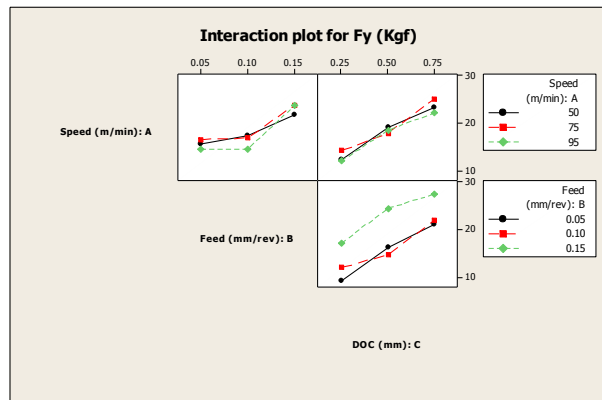
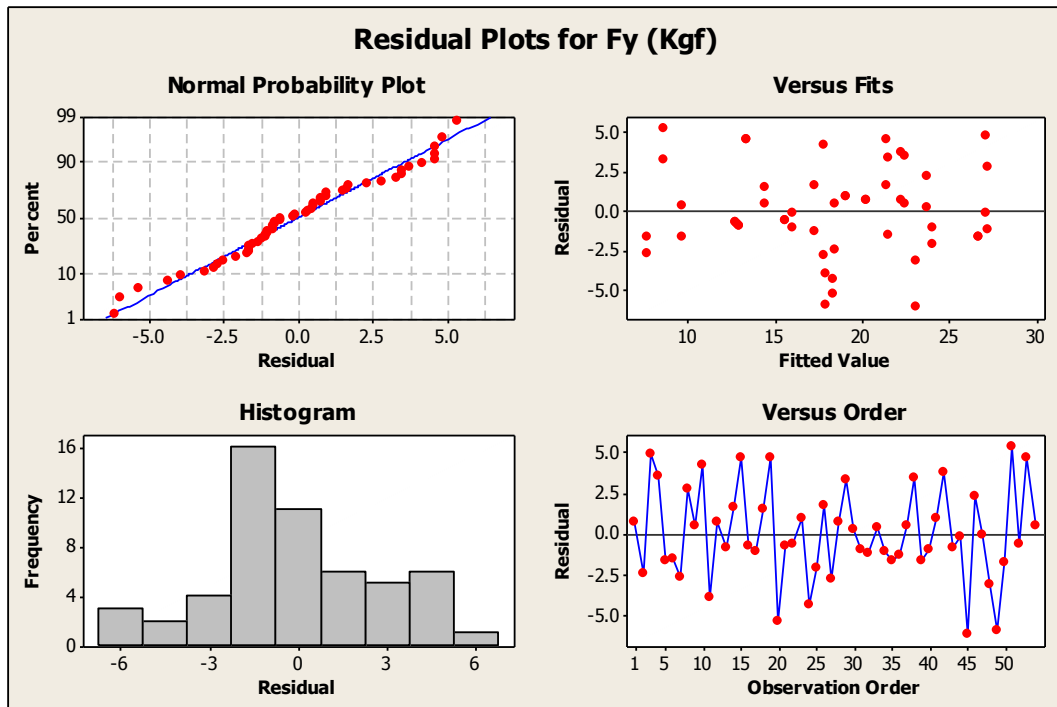
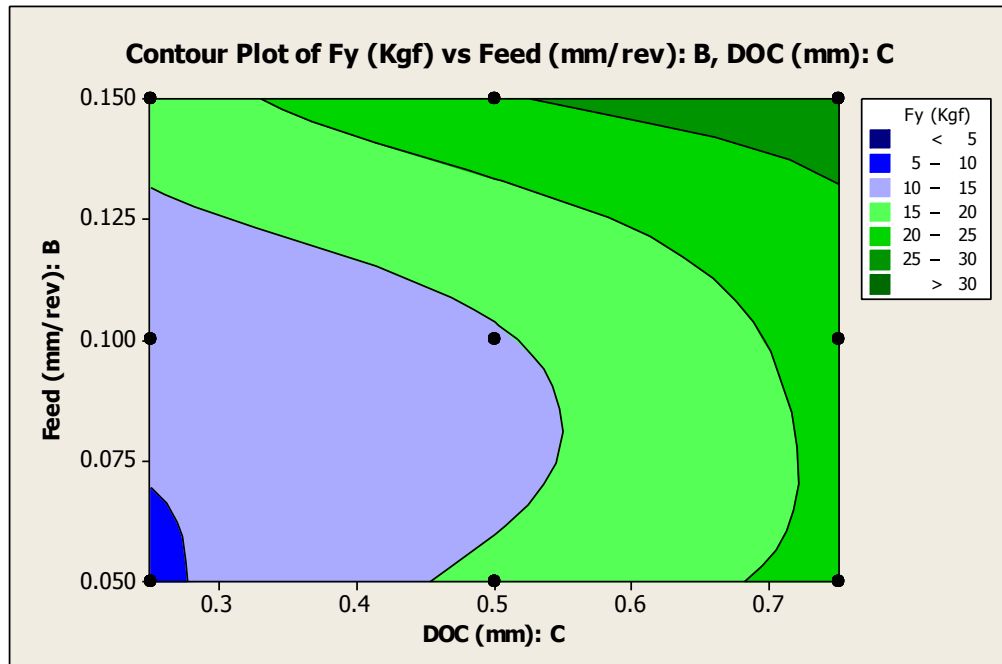


Figure - 2: Interaction Plot for Cutting Force  $F_c$ .

Figure - 3: Residual Plot for Cutting force  $F_y$  (kgf.)

The power consumption minimization was also one of the objectives of this research. So, having observed through the analysis of variance that feed rate and depth of cut have significant influence on the cutting force which in turn has bearing on the power consumption, the contour plot was developed. It can be observed that for power consumption minimization, the focus should be on choosing an appropriate combination of feed rate ( $< 0.06$  mm/rev) and depth of cut ( $< 0.15$  mm) (figure 4).

Figure - 4: Contour Plot for Cutting force  $F_y$  (kgf.).

#### 4.2. Surface roughness analysis

The surface roughness analysis of variance (Table 5; figure 5) indicates that the hypothesis  $H_4$  stands supported which claims that feed rate has significant influence on surface roughness. Further, among the interaction effects, interaction between speed and feed has significant influence on surface finish (figure 6). R-square of 84.25% indicates a good model fit, but R-square adjusted of 60.09% is slightly on the lower side of goodness of fit, but in the acceptable limit (figure 7).

Table - 5: ANOVA for Surface Roughness

Source	DF	Seq SS	Adj SS	Adj MS	F	P	Hypothesis
Speed	2	3.50	3.50	1.75	1.63	0.215	--
Feed	2	107.30	107.30	53.65	49.88	0.000*	Supported
DOC	2	0.52	0.52	0.26	0.24	0.79	--
Speed*Feed	4	19.17	19.17	4.79	4.46	0.01*	Supported
Speed*DOC	4	7.23	7.23	1.81	1.68	0.18	--
Feed*DOC	4	6.27	6.27	1.57	1.46	0.24	--
Speed*Feed*DOC	8	11.37	11.37	1.42	1.32	0.28	--
Error	27	29.04	29.04	1.08	--	--	
Total	53	184.40	--	--	--	--	
<b>S = 1.037</b>		<b>R-Sq = 84.25%</b>		<b>R-Sq(adj) = 69.09%</b>			

\*Significant influence ( $\alpha = 0.05$ ).

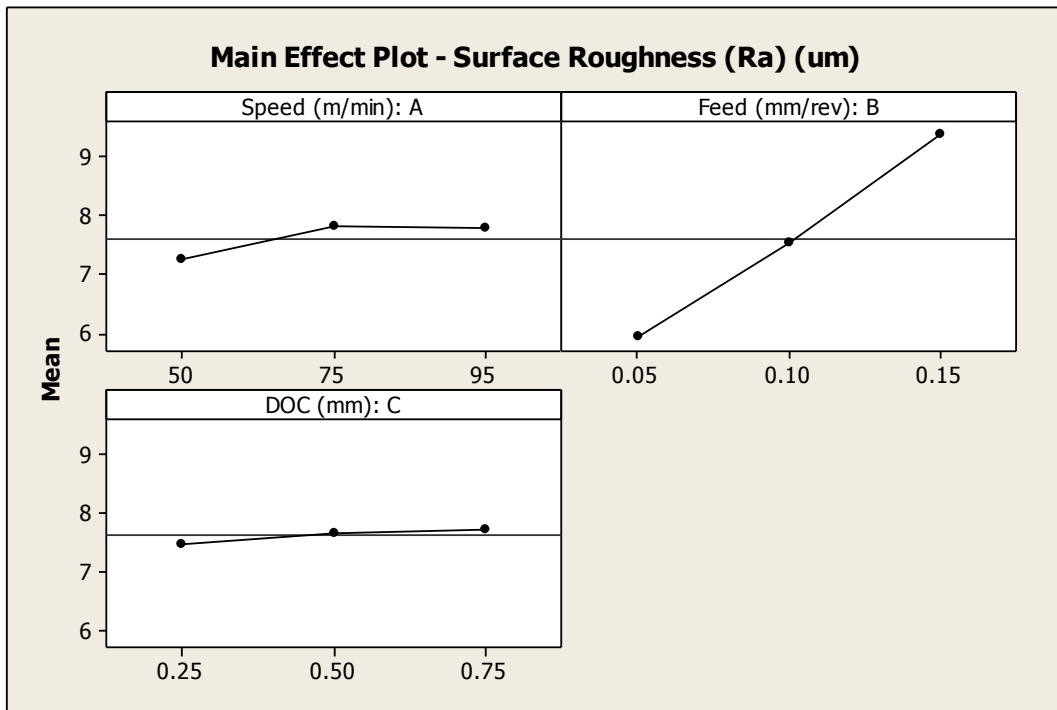
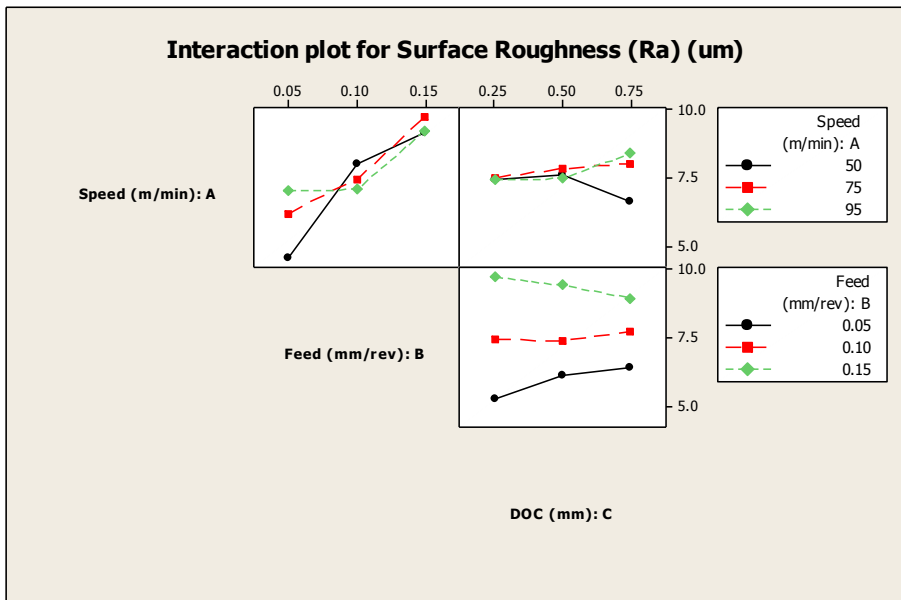
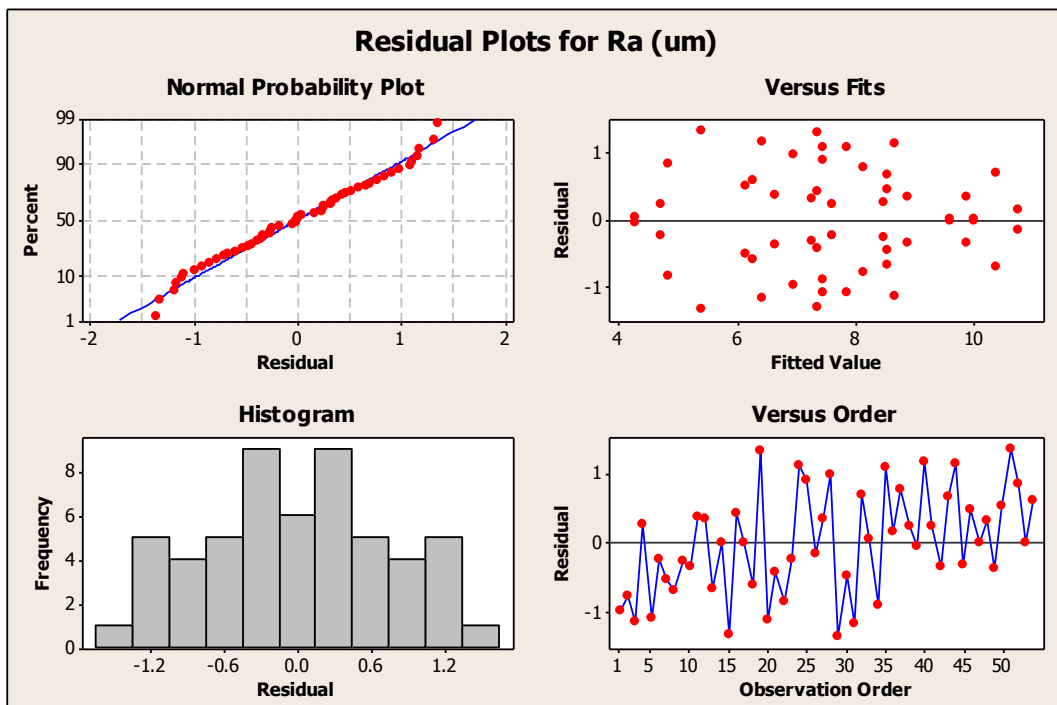


Figure - 5: Main Effects Plot for Surface Roughness  $R_a$  ( $\mu\text{m}$ )

Figure - 6: Interaction Plot for Surface Roughness  $R_a(\mu\text{m})$ Figure - 7: Residual Plot for Surface Roughness  $R_a (\mu\text{m})$ 

The regression analysis was carried out to study the influence of cutting parameters on surface roughness and develop the regression model with interaction effects (Table 6). The model is adequately a good fit ( $R^2 = 79.4\%$ ;  $R^2 \text{ adjusted} = 76.3\%$ ). The regression equation is as follows. It is interesting to note that all the cutting parameters as well as the interaction effects as indicated in the table 6 seem to be significantly influencing the surface roughness.

$$Ra (\mu\text{m}) = -1.86 + 0.0743 * \text{Speed} + 110 * \text{Feed} + 5.48 * \text{depth of cut} - 0.116 * \text{speed*feed} - 60.1 * \text{feed*depth of cut} + 0.0930 * \text{speed*feed*depth of cut} + \epsilon$$

Where,  $\epsilon$  = regression error

Table - 6: Regression Analysis (Surface Roughness)

Predictor	Coef	SE Coef	T	P
Constant	-1.86	1.89	-0.98	0.33
Speed	0.074	0.03	2.83	0.01
Feed	110.42	19.49	5.66	0.00
DOC	5.48	2.39	2.29	0.026
Speed*Feed	-0.12	0.04	-3.32	0.002
Feed*DOC	-60.14	19.28	-3.12	0.003
Speed*Feed*DOC	0.09	0.04	2.21	0.032
<b>S = 2.98097 R-Sq = 79.4% R-Sq(adj) = 76.3%</b>				

## 5. Discussions and conclusions

The feed rate has significant influence on both the cutting force and surface roughness. Cutting Speed has no significant effect on the cutting force as well as the surface roughness. Depth of cut has a significant influence on cutting force, but has an insignificant influence on surface roughness. The interaction of feed and depth of cut and the interaction of all the three cutting parameters have significant influence on cutting force, whereas, none of the interaction effects are having significant influence on the surface roughness produced. Hence, in the turning process optimization with respect to power consumption, the focus should be on choosing an appropriate combination of feed rate ( $< 0.06$  mm/rev) and depth of cut ( $< 0.15$  mm). In comparison to the sequential approach adopted in most of the contemporary research, this research has shown that adjusted approach can also be successfully used to fit a reasonably acceptable and generalized model provided, it is a mono-block design.

The surface roughness is a very important parameter as indicated before because it has bearing on several other usage related issues of the component. The regression model has made certain key revelation in terms of the influence of cutting parameters, which has not been revealed in the analysis of variance. The regression model with the P values indicated that the three cutting parameters and the two level interaction of speed & feed and feed & depth of cut, as well as the third level interaction of all the three have significant influence on surface roughness. The most significant among all these is obviously the feed rate which is very much in agreement with the analysis of variance. This is anticipated as it is well known that for a given tool nose radius, the theoretical surface roughness ( $R_a = f^2 / (32 \times r)$ ) is mainly a function of the feed rate [6].

While the results declared through this experimental work may be generalized to a considerable extent while working on hardened AISI 1050 steel using ceramic (KY1615) tool, the study is limited to the extreme range of values of the cutting parameters specified. Future research work may be directed towards applying Response Surface Methodology to further fine tune the optimization of cutting parameters, which was beyond the scope of this research, as it was mainly focussed towards the identification of most significantly influencing factors.

## References

- [1] Narutaki, N., Yamane, Y., Okushima, K., 1979. Tool wear and cutting temperature of CBN tool in machining of hardened steels. Ann. CIRP 28 (1), 23–28.
- [2] Hodgson, T., Trendler, P., Ravignani, G., 1981. Turning hardened tool steels with cubic boron nitride inserts. Ann. CIRP 30 (1), 63–66.
- [3] Konig, W., Komanduri, R., Tonshoff, H., Ackershoff, G., (1984), Machining of hard materials. Ann. CIRP 33 (2), 417–428.
- [4] Tonshoff, H.K., Arendt, C., Amor, R.B., 2000. Cutting hardened steel. Ann. CIRP 49 (2), 1–19.
- [5] Lalwani, D.I., Mehta, N.K., & Jain, P.K. (2008), “Experimental investigations of cutting parameters influence on cutting forces and surface roughness in finish hard turning of MDN250 steel”, *Journal of materials processing technology*, vol. 206, pp. 167–179.
- [6] Shaw, M.C., 1984. Metal Cutting Principles. Oxford University Press, Oxford, NY.
- [7] Özel T. and Karpat Y., (2005), “Predictive modeling of surface roughness and tool wear in hard turning using regression and neural networks”, *International Journal of Machine Tools and Manufacture*, Volume 45, pp. 467–479.
- [8] Groover M. P., (1996), Fundamentals of Modern Manufacturing, Prentice-Hall, Upper Saddle River, NJ (now published by John Wiley, New York), p. 634.
- [9] Kalpakjian S. and Schmid S. R., (2008), Manufacturing Processes for Engineering Materials, 5<sup>th</sup> ed., Pearson Education, Inc., SBN 9-78013227-271-1.
- [10] Aruna M., Dhanalakshmi V., (2010), Response surface methodology in finish turning INCONEL 718, *International Journal of Engineering Science and Technology*, vol. 2, no. 9, pp. 4292-4297.
- [11] Fang, X.D., Safi-Jahanshaki, H., (1997), A new algorithm for developing a reference model for predicting surface roughness in finish machining of steels. *Int. J. Prod. Res.* 35 (1), 179–197.
- [12] Thiele, J.D., Melkote, S.N., 1999. Effect of cutting edge geometry and work-piece hardness on surface generation in the finish hard turning of AISI

- 52100 steel, *Journal of material processing technology*, vol. 94, pp. 216–226.
- [13] Chen, W., (2000), Cutting forces and surface finish when machining medium hardness steel using CBN tools. *Int. J. Mach. Tools Manuf.* 40, 455–466.
- [14] Darwish, S.M., 2000. The impact of the tool material and the cutting parameters on surface roughness of supermet 718 nickel superalloy. *J. Mater. Process. Technol.* Vol. 97, pp. 10–18.
- [15] Feng C. X. (Jack) and Wang X., (2002), “Development of Empirical Models for Surface Roughness Prediction in Finish Turning”, *International Journal of Advanced Manufacturing Technology*, Volume 20, pp. 348–356.
- [16] Kopa C. J., Bahor, M., Sokovi C. M., (2002), Optimal machining parameters for achieving the desired surface roughness in fine turning of cold pre-formed steel work-pieces. *International Journal of Machine Tools Manufacturing*, vol. 42, pp. 707–716.
- [17] Lin W. S., Lee B. Y., Wu C. L., (2001), “Modeling the surface roughness and cutting force for turning”, *Journal of Materials Processing Technology*, Vol. 108, pp. 286–293.
- [18] Suresh P. V. S., Rao P. V. and Deshmukh S. G., (2002), “A genetic algorithmic approach for optimization of surface roughness prediction model”, *International Journal of Machine Tools and Manufacture*, Volume 42, pp. 675–680.
- [19] Lee S. S. and Chen J. C., (2003), “Online surface roughness recognition system using artificial neural networks system in turning operations” *International Journal of Advanced Manufacturing Technology*, Volume 22, pp. 498–509.
- [20] Kirby E. D., Zhang Z. and Chen J. C., (2004), “Development of An Accelerometer based surface roughness Prediction System in Turning Operation Using Multiple Regression Techniques”, *Journal of Industrial Technology*, Volume 20, Number 4, pp. 1-8.
- [21] Kohli A. and Dixit U. S., (2005), “A neural-network-based methodology for the prediction of surface roughness in a turning process”, *International Journal of Advanced Manufacturing Technology*, Volume 25, pp.118–129.
- [22] Pal S. K. and Chakraborty D., (2005), “Surface roughness prediction in turning using artificial neural network”, *Neural Computing and Application*, Volume 14, pp. 319–324.
- [23] Singh H. and Kumar P., (2006), “Optimizing Feed Force for Turned Parts through the Taguchi Technique”, *Sadhana*, Volume 31, Number 6, pp. 671–681.
- [24] Ahmed S. G., (2006), “Development of a Prediction Model for Surface Roughness in Finish Turning of Aluminium”, *Sudan Engineering Society Journal*, Volume 52, Number 45, pp. 1-5.
- [25] Zhong Z. W., Khoo L. P. and Han S. T., (2006), “Prediction of surface roughness of turned surfaces using neural networks”, *International Journal of Advance Manufacturing Technology*, Volume 28, pp. 688–693.
- [26] Doniavi A., Eskanderzade M. and Tahmesebian M., (2007), “Empirical Modeling of Surface Roughness in Turning Process of 1060 steel using Factorial Design Methodology”, *Journal of Applied Sciences*, Volume 7, Number17, pp. 2509-2513.
- [27] Kassab S. Y. and Khoshnaw Y. K., (2007), “The Effect of Cutting Tool Vibration on Surface Roughness of Work piece in Dry Turning Operation”, *Engineering and Technology*, Volume 25, Number 7, pp. 879-889.
- [28] Al-Ahmari A. M. A., (2007), “Predictive machinability models for a selected hard material in turning operations”, *Journal of Materials Processing Technology*, Volume 190, pp. 305–311.
- [29] Wang M. Y. and Lan T. S., (2008), “Parametric Optimization on Multi-Objective Precision Turning Using Grey Relational Analysis”. *Information Technology Journal*, Volume 7, pp.1072-1076.
- [30] Sahoo P., Barman T. K. and Routara B. C., (2008), “Taguchi based practical dimension modeling and optimization in CNC turning”, *Advance in Production Engineering and Management*, Volume 3, Number 4, pp. 205-217.
- [31] Reddy B. S., Padmanabhan G. and Reddy K. V. K., (2008), “Surface Roughness Prediction Techniques for CNC turning”, *Asian Journal of Scientific Research*, Volume 1, Number 3, pp. 256-264.
- [32] Thamma R., (2008), “Comparison between Multiple Regression Models to Study Effect of Turning Parameters on the Surface Roughness”, *Proceedings of the 2008, 96 IAJC-IJME International Conference*, ISBN 978-1-60643-379-9, Paper 133, ENG 103 pp. 1-12.
- [33] Fnides B., Aouici H., Yallese M. A., (2008), “Cutting forces and surface roughness in hard turning of hot work steel X38CrMoV5-1 using mixed ceramic”, *Mechanika*, Volume 2, Number 70, pp. 73-78.
- [34] Zawada-Tomkiewicz, A. (2011), Analysis of surface roughness parameters achieved by hard turning with the use of PCBN tools, *Estonian Journal of Engineering*, vol. 17, no. 1, pp. 88–99.
- [35] Davis, R. (2012), Optimization of Surface Roughness In Wet Turning Operation Of En24 Steel, *International Journal of Mechanical and Production Engineering Research and Development (IJMPERD )*, Vol.2, Issue 3, pp. 28-35.
- [36] Lazarevića, D., Madića, M., Jankovića, P. Lazarević, A., (2012), Cutting Parameters Optimization for Surface Roughness in Turning Operation of Polyethylene (PE) Using Taguchi Method, vol. 34, no. 2, pp. 68-73.

## MTT ACTIVITY -07

### PRODUCTION DRAWING LIMITS, FITS AND TOLERANCE

#### Limit system

There are three terms used in the limit system:

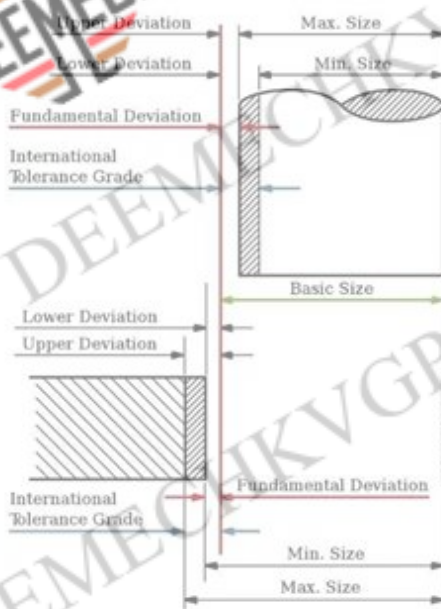
1. **Tolerance:** Deviation from a basic value is defined as Tolerance. It can be obtained by taking the difference between the maximum and minimum permissible limits.
2. **Limits:** Two extreme permissible sizes between which the actual size is contained are defined as limits.
3. **Deviation:** The algebraic difference between a size and its corresponding basic size. There are two types of deviations: 1) Upper deviation 2) Lower deviation

The fundamental deviation is either the upper or lower deviation, depending on which is closer to the basic size.

#### Tolerances

Due to human errors, machine settings, etc., it is nearly impossible to manufacture an absolute dimension as specified by the designer. Deviation in dimensions from the basic value always arises. This deviation of dimensions from the basic value is known as Tolerance.

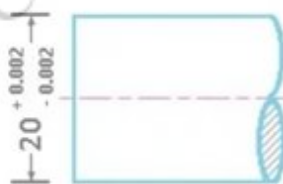
The figure shows mechanical tolerances which occur during operations.



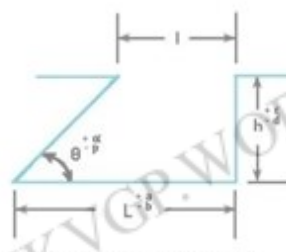
#### ENGINEERING TOLERANCE



UNILATERAL TOLERANCE



BILATERAL TOLERANCE



COMPOUND TOLERANCE

## *Fits*

The relation between two mating parts is called **fit**. Depending upon the actual limits of the hole or shaft sizes, fits may be classified as clearance fit, transition fit and interference fit.

### *Clearance fit*

Clearance fit is defined as a clearance between mating parts. In clearance fit, there is always a positive clearance between the hole and shaft.

### *Transition fit*

Transition fit may result in either an interference or clearance, depending upon the actual values of the tolerance of individual parts.

### *Interference fit*

Interference fit is obtained if the difference between the hole and shaft sizes is negative before assembly. Interference fit generally ranges from minimum to maximum interference. The two extreme cases of interference are as follows:

#### *Minimum interference*

The magnitude of the difference (negative) between the maximum size of the hole and the minimum size of the shaft in an interference fit before assembly.

#### *Maximum interference*

The magnitude of the difference between the minimum size of the hole and the maximum size of the shaft in an interference or a transition fit before assembly.

## **Hole Basis and shaft basis system:**

In identifying limit dimensions for the three classes of fit, two systems are in use:

1. *Hole basis system:* The size of the shaft is obtained by subtracting the allowance from the basic size of the hole. Tolerances are then applied to each part separately. In this system, the lower deviation of the hole is zero. The letter symbol indication for this is 'H'.
2. *Shaft basis system:* The upper deviation of the shaft is zero, and the size of the hole is obtained by adding the allowance to the basic size of the shaft. The letter symbol indication is 'h'.

## Analyze surface finish symbols in a Production Drawing

### Surface Finish and Surface Roughness

The finish on a metal surface after machining depends mainly on the material and some are as follows.

- It depends on the structure of the metal before and after machining,
- Depends on cutting conditions such as type and degree of sharpness of the cutting tool,
- Depth of cut,
- Amount of feed,
- Coolant used,
- Working conditions such as hot or cold,
- Vibrations and deflections of the tool or the workpiece while cutting, etc.

### Symbols for Indicating Surface Finish

- The quality of a surface finish on a metal surface produced by production method other than machining is shown on the drawing by a tick symbol as shown in figure-A.
- This basic symbol consists of two legs of unequal length.
- These are inclined at approximately 60 degrees to the line representing the surface to be machined with the vertex touching it.

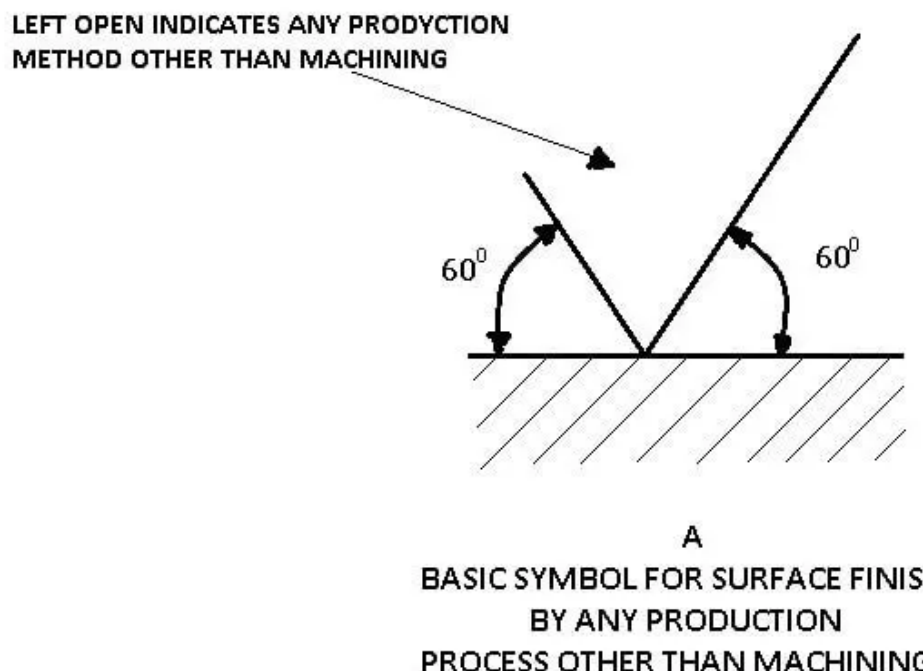


figure-A.

- If the surface finish is to be obtained by removing the material by any machining process, a horizontal bar is to be added to the basic symbol.
- Converting it into an equilateral triangle as shown in figure-B.

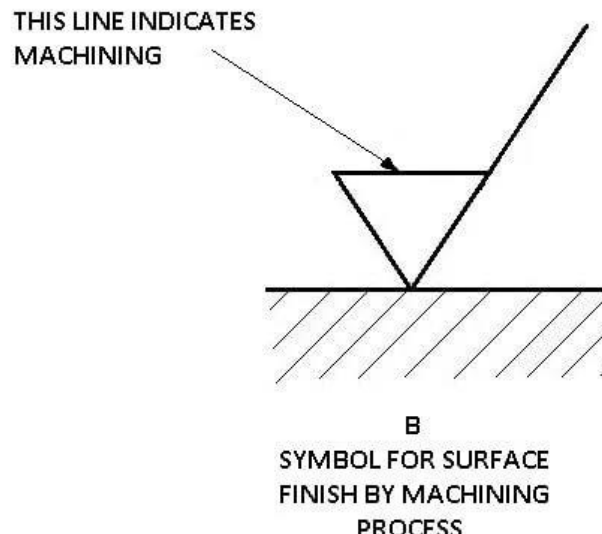


figure-B.

- If the surface is to be produced without removal of material or when a surface is to be left in the very state resulting from the other manufacturing process, whether this state was achieved by the removal of the material or otherwise, a circle is written in the basic symbol as shown in figure-C.

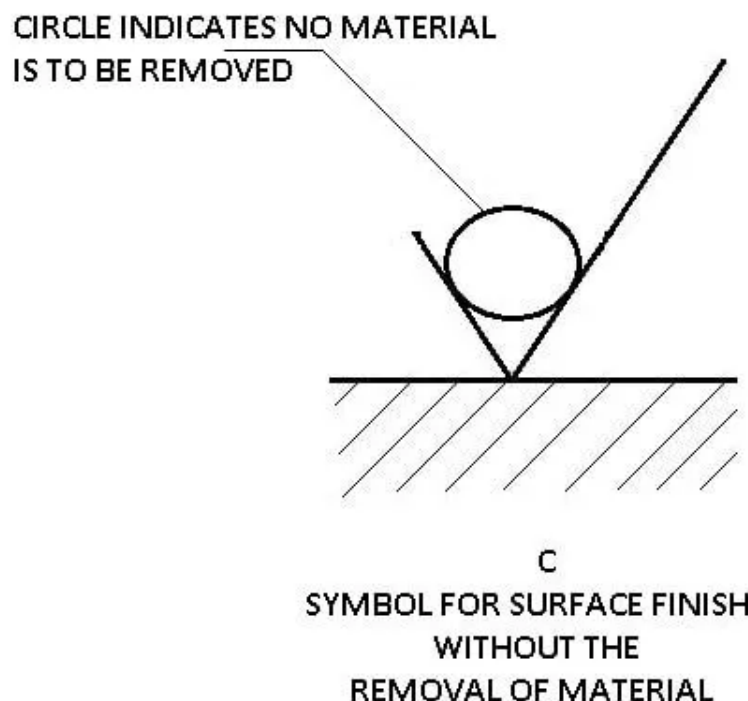


figure-C.

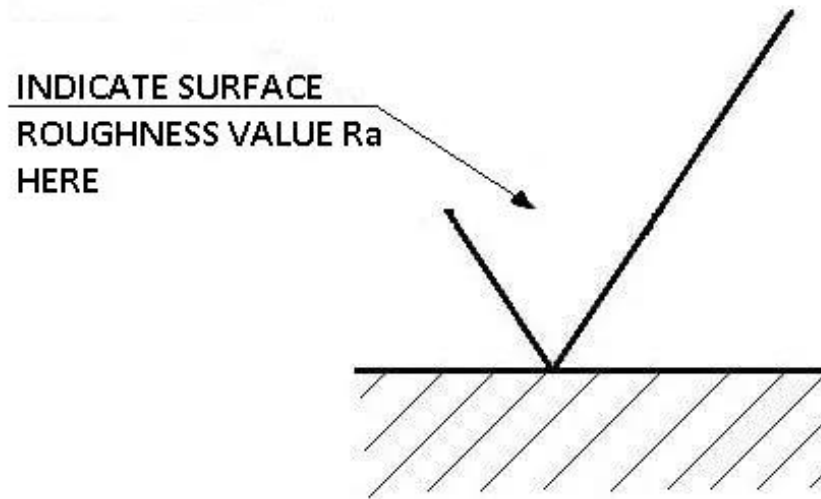
- If the general manufacturing processes by themselves ensure achieving of the acceptable surface finish, then the specification of the surface finish is unnecessary, hence need not be indicated.

### Indication of Surface Roughness Values

The surface roughness may be indicated in the basic symbol shown in the above figures by

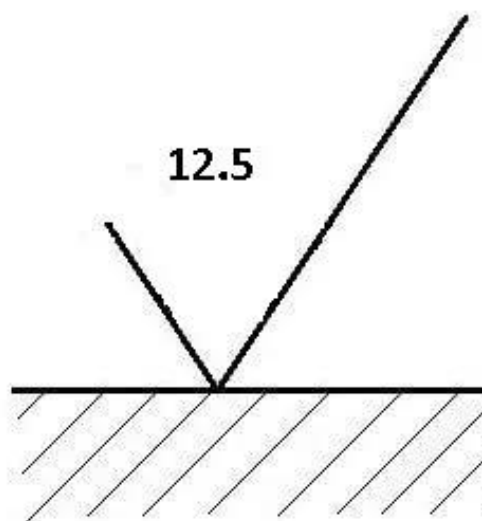
- Roughness value in a micrometre
- Roughness grade numbers, or
- By triangle symbol

The indication of surface roughness values in the surface finish symbols are shown the figure A.



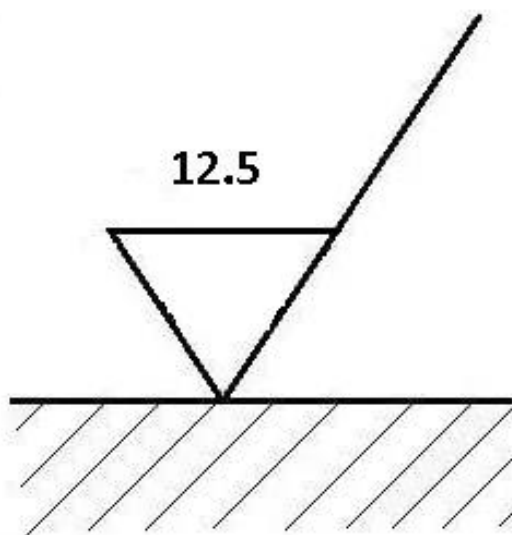
(A)

a) If the surface roughness is obtained by any production method other than machining, the value of surface rough necessary say,  $12.5\mu\text{m}$  is indicated in the basic symbol as shown in figure B.



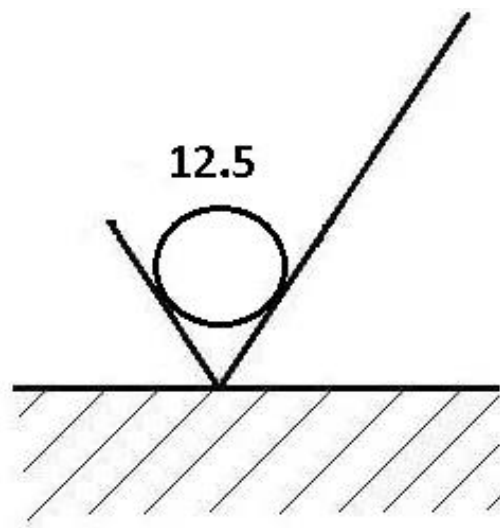
(B)

- b) If the surface roughness is obtained by removing the material by machining, the value of surface roughness, say  $12.5\mu\text{m}$ , should be indicated as shown in figure C.



(C)

- c) If the surface roughness is to be obtained without the removal of material or when it results from the previous production process, the value of surface roughness say  $12.5\mu\text{m}$ , should be indicated as shown in figure D.



(D)

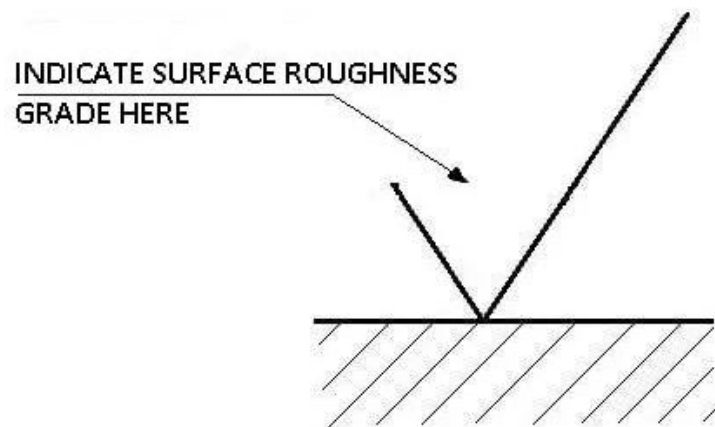
### Indication of Surface Roughness Grades

- The surface roughness is too shown by the grade number instead of their numerical values. The BIS has prescribed twelve grades of surface roughness.
- These grades of surface roughness.
- These grades of surface roughness are numbered as N1, N2, N3.....N12.
- The standard prescribed grades of surface roughness may be chosen from the given Table-A corresponding to the required surface roughness values.

**Table-A: Surface Roughness, Values, Grades and Symbols**

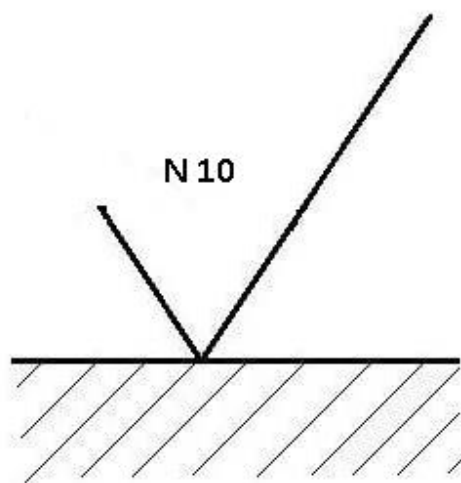
Roughness Value Ra $\mu\text{m}$	Roughness Grade Number	Roughness Symbols
50	N 12	$\cong$
25	N 11	$\nabla$
12.5	N 10	
6.3	N 10	
3.2	N 9	$\nabla\nabla$
1.6	N 8	
0.8	N 6	$\nabla\nabla\nabla$
0.4	N 5	
0.2	N 4	
0.1	N 3	
0.05	N 2	$\nabla\nabla\nabla\nabla$
0.025	N 1	

- When the quality of surface finish is to be indicated by the roughness grade number in the surface finish symbol, the grade number is written in the same place of the roughness value the Figure-A.



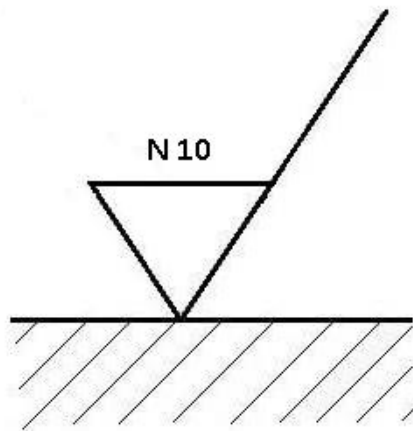
(A)

- a) If the surface roughness is obtained by any production method other than machining, the grade number of surface roughness, for example, N10, is indicated in the basic symbol as shown in Figure-B.



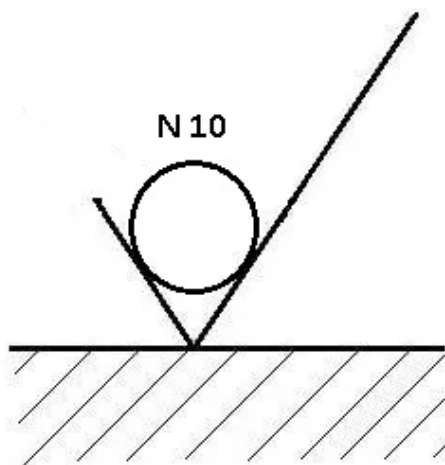
(B)

b) If the surface roughness is obtained by removing the material by machining the grade number of surface roughness, for example, N10 is indicated as shown in Figure-C.



(C)

c) If the surface roughness is to be obtained without the removal of material or when it results from the previous production process, the value of the surface roughness, for example, N10 should be indicated as shown in Figure-D.

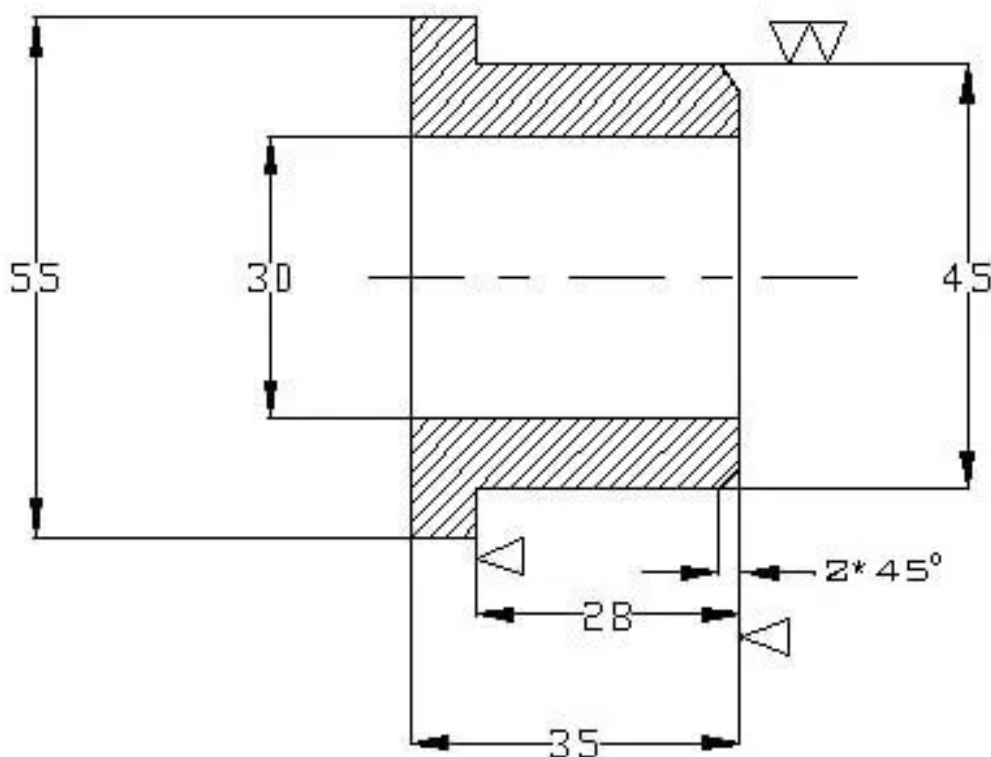


(D)

### Indication of Surface Roughness by Triangle Symbol

- The BIS (Bureau of Indian Standards) prefers the sign of surface roughness either by grades or by values, from the point of the requirements of overall engineering industries.
- It is suggested to indicate the surface roughness on drawing by symbols.
- The BIS recommended symbols for indicating the surface finish are shown in Table A.
- For the roughness values greater than  $25\mu\text{m}$ , the symbol is used. For roughness value less than  $25\mu\text{m}$ , the equilateral triangular symbol is used.

### Indication of Surface Roughness by Symbols

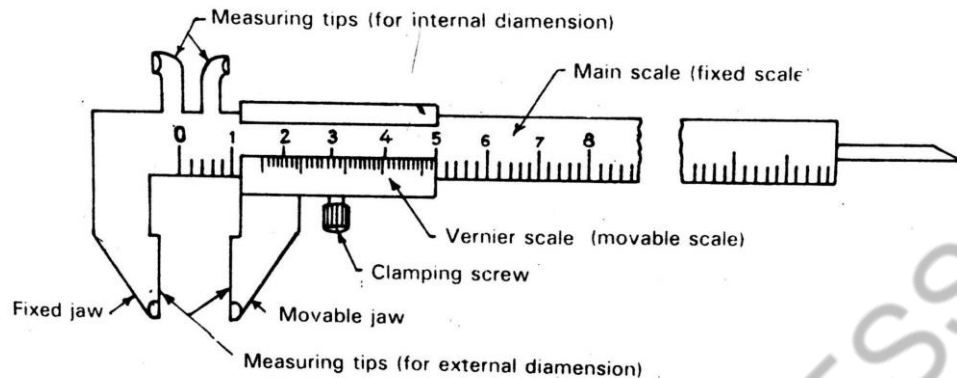


The number triangles indicate the range of surface roughness. As recommended in Table A, for roughness values ranging from  $12\mu\text{m}$  to  $25\mu\text{m}$  a single triangle is used.

- For roughness values ranging from  $1.6$  to  $6.3\mu\text{m}$ , two triangles are used in series.
- For roughness values ranging from  $0.025\mu\text{m}$  to  $0.1\mu\text{m}$ , four triangles are used in series.
- The figure shows a typical example of indicating the surface finish by symbols.

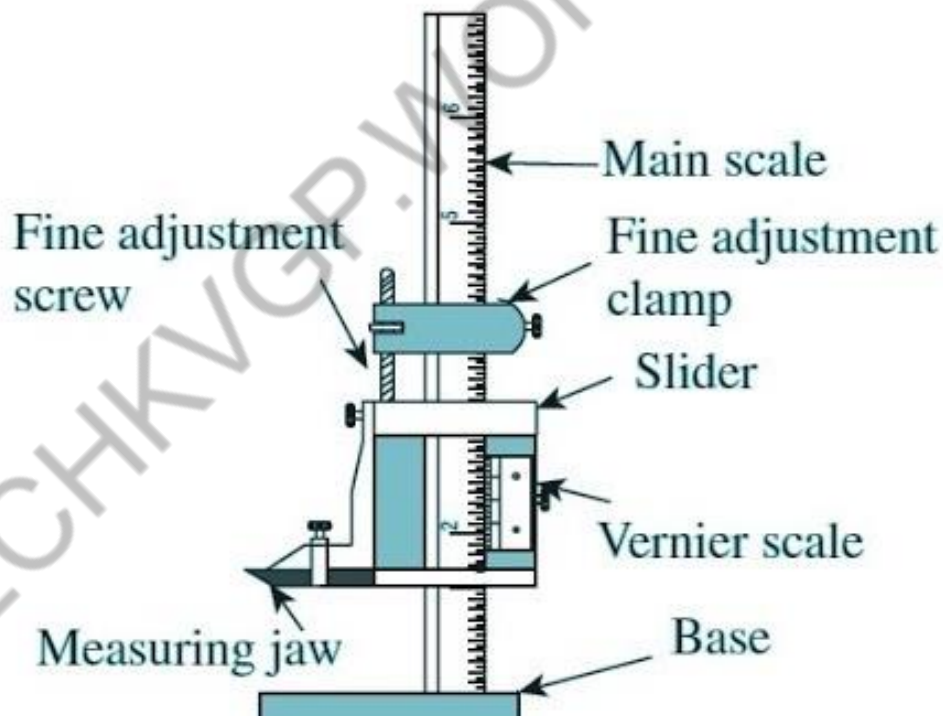
## Demonstrate the various measuring instruments used in Machine Shop

### 1. Vernier Caliper:



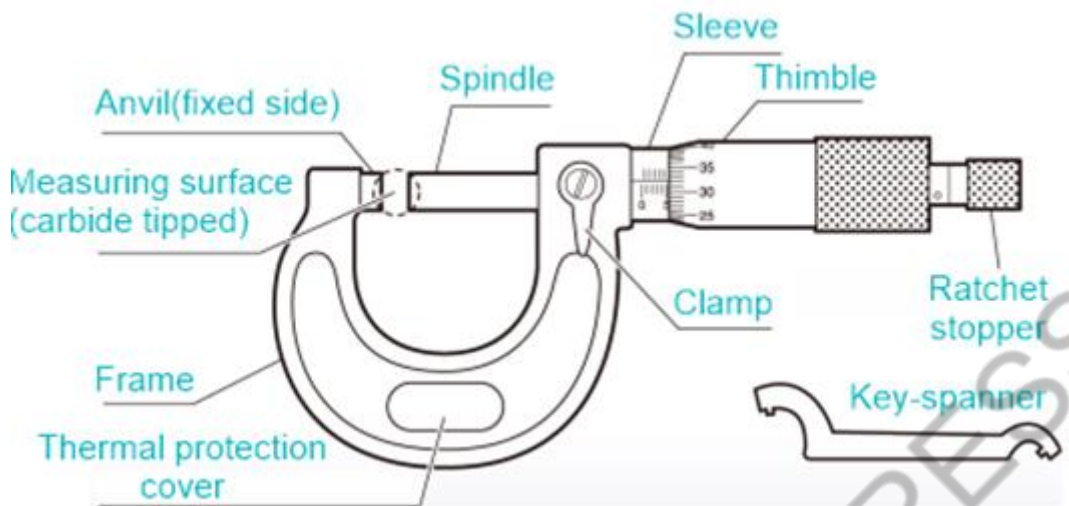
- We know the core use of Vernier Calipers is for measuring the distance between two opposite sides of a surface.
- We can measure the internal and external dimensions and even the height of an object with accuracy. It can measure up to one-hundredth of a millimeter.

### 2. Vernier Height Gauge:



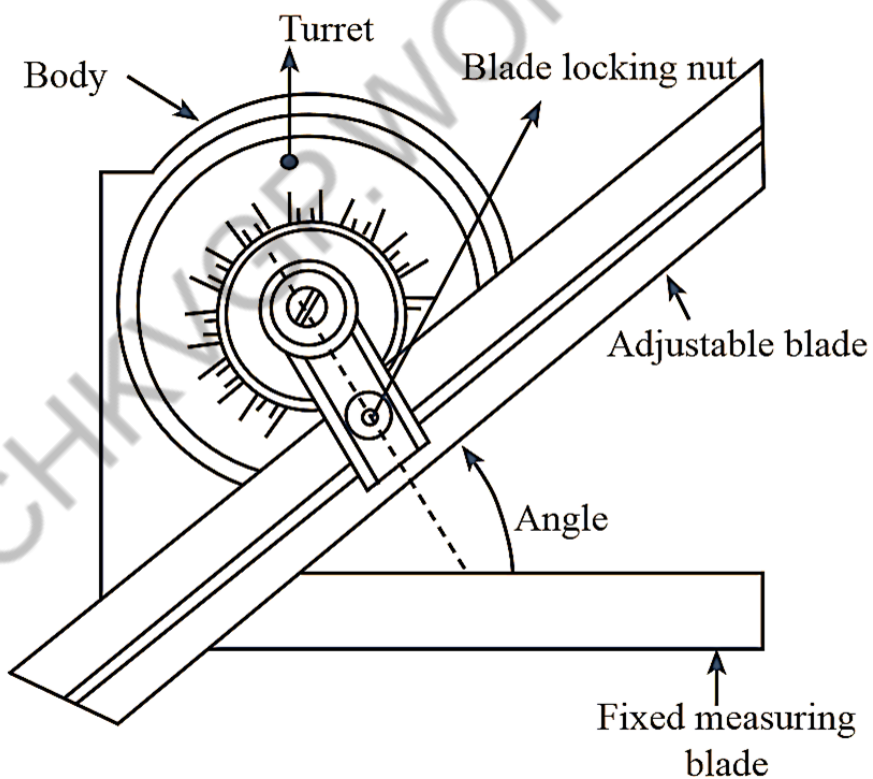
- Vernier height gauges are used in metrology and metalworking to detect or measure vertical distances.
- The height gauges are often used to measure a granite surface or scribe part features from a datum plane.

### 3. Micrometer:



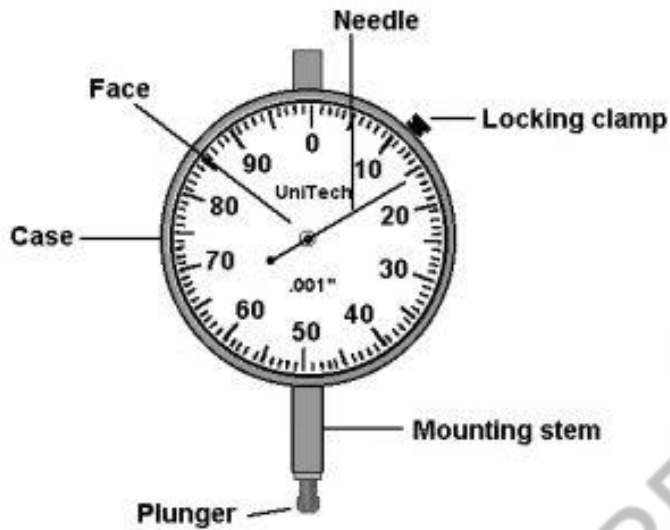
- A micrometer is an instrument used for making precise linear measurements of dimensions such as diameter, thickness, and lengths of solid bodies

### 4. Universal bevel protractor:



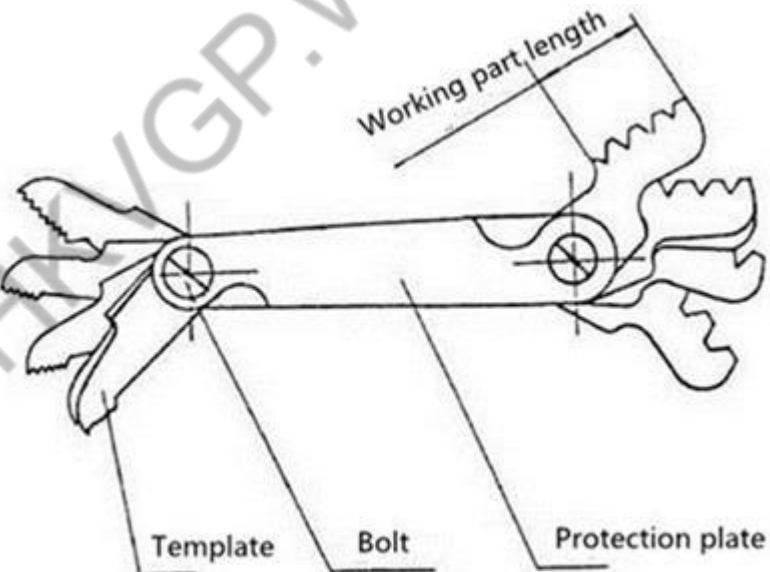
- Universal bevel protractors are also used by toolmakers; as they measure angles by mechanical contact they are classed as mechanical protractors.

## 5. Dial Gauge:



- Dial gauge or also known as a dial indicator, is a comparison measuring instrument (comparator).
- This tool is used to measure a workpiece's flatness of surface, roundness, runout, and so on.
- The working principle of the dial gauge is dependent on the movement of the spindle.

## 6. Thread Gauges:



- A thread gauge is used to check the dimensions of a specific thread form angle, pitch and diameter.

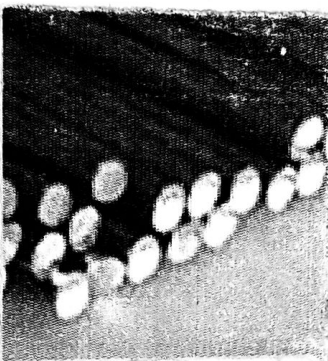
## Activity - 10

collect the sample piece of various raw material used in machine shop and discuss their mechanical chemical and physical properties.

Various raw material are used in machine shop. they are.

\* cast Iron

\* mild steel.



cast Iron =>

cast iron is an eutectic alloy of iron and carbon. It has relatively low melting point therefore it can be melted very easily. It requires less fuel.

and more easily operated in furnaces. The carbon content of the cast iron varies from 2% to 4.5%. It also contains small amounts of silicon sulphur, manganese and phosphorus.

The molten metal of cast iron easily fills in intricate moulds completely and easily.

Types of cast Iron =>

Following are the important types of cast iron.

i) white cast iron =>

It is a particular variety of cast iron which shows a white fracture. It has following

compositions They are carbon - 2.1% to 2.3%. manganese 0.1% to 0.4%, and silicon - 0.85% to 1.2%. phosphorus - 0.5% to 0.2%, sulphur - 0.12% to 0.35% and remaining is iron.

### 2) Gray cast iron

It is an ordinary commercial cast iron & it has the following compositions They are carbon - 3% to 3.5%, manganese - 0.4% to 1%, silicon 1% to 2.75%, phosphorus 0.15% to 1%, sulphur 0.02% to 0.15% and remaining is iron.

### 3) Nodular cast iron

The nodular cast iron is also known as ductile cast iron spheroidal graphite cast iron or high strength cast iron. It is produced by adding magnesium to the molten cast iron. The magnesium converts the graphite of cast iron from flake form to spheroidal form thereby improving its mechanical properties considerably.

### 4) malleable cast iron

The malleable cast iron is obtained from white cast iron by a suitable heat treatment process i.e. by annealing. The annealing process separates the combined carbon of the white cast iron into nodules of free graphite.

## Physical properties of metals or cast iron $\Rightarrow$

- 1) Melting point  $\Rightarrow$  It can be melt easily. It's melting point about  $1200^{\circ}\text{C}$
- 2) Density  $\Rightarrow$  Density of cast iron is 6800 to 7800 kg per meter cube.
- 3) Shape  $\Rightarrow$  The shape of metal may be round, square, hexagonal, octagonal, strip, sheet, angle channel, round tubes and square tubes etc.
- 4) Size  $\Rightarrow$  It is the overall dimensions of a cast iron.
- 5) Colour  $\Rightarrow$  Colour is the physical property of a metal or a cast iron of displaying a particular hue in the normal daylight.
- 6) Lustre  $\Rightarrow$  Lustre is the property of brightness of a surface of a metal.
- 7) specific gravity  $\Rightarrow$  At the 7.2 ratio density of a metal to the density of water at a specified temperature.
- 8) Porosity  $\Rightarrow$  The higher carbon content of cast iron means that it solidifies as a heterogeneous alloy and therefore has more than one micro crystalline structure present in the material.

mechanical properties of cast iron  $\Rightarrow$

1) Elasticity  $\Rightarrow$  In cast iron the elasticity is normally high and sometimes low.

2) plasticity  $\Rightarrow$  It is the property of the metal which a metal takes place permanent deformation without fracture. In cast iron good plasticity it can take permanent deformation without fracture ex: rolling forging etc.

3) Ductility  $\Rightarrow$  The cast iron can be easily drawn into wires or elongated before rupture takes places.

4) Brittleness  $\Rightarrow$  cast iron is a brittle material.

5) Hardness  $\Rightarrow$  cast iron is cannot absorb maximum energy compared to other metals.

6) Toughness  $\Rightarrow$  compared to other metals the cast iron cannot absorb maximum energy before fracture.

7) Stiffness  $\Rightarrow$  In cast iron the property which a metal will not deform or deflect when load is applied very poor because the cast iron not a hard material.

8) Resilience  $\Rightarrow$  cast iron cannot resist any shocks or impact loads because it is a brittle materials.

9) Malleability  $\Rightarrow$  The cast iron can be hammered in to thin sheets because it has a character plasticity.

10) Creep  $\Rightarrow$  The cast iron deforms continuously and slowly under steady load.

11) Endurance  $\Rightarrow$  The endurance limit of high-strength cast iron was 170 MPa. It can withstand varying stress at this tension.

Chemical properties of cast iron  $\Rightarrow$

- 1) Cast irons typically contain 2-4 wt% of carbon with a high silicon concentration and a greater concentration of impurities than steels.
- 2) The carbon equivalent of a cast iron helps to distinguish the grey irons which cool into a microstructure containing graphite.
- 3) The white irons where the carbon is present mainly as cementite. Therefore it is extremely hard.
- 4) A high cooling rate and low carbon equivalent favours the formation of white-cast iron.
- 5) Low cooling rate or high carbon equivalent promotes grey cast iron.
- 6) Grey cast iron are softer with a microstructure of graphite in transformed austenite and cementite matrix.
- 7) The sulphur in cast irons is known to favor the formation of graphite flakes. Therefore cast iron have a good damping and good machinability characteristics.

mild steel ⇒

mild steel or low carbon steel also known as plain carbon steel. It can be defined as a steel which has properties mainly due to its carbon content and does not contain more than 0.5% of silicon and 1.5% of manganese. The plain carbon steels contains the carbon varying from 0.06% to 1.4%. These steels are strong, tough, ductile and used in expensive material. They can be cast worked, machined and heat treated to a wide range of properties.

They of plain carbon steels and their compositions. They are ⇒

- 1) Dead mild steel ⇒ 0.06% to 0.12% carbon.
- 2) Low carbon steel ⇒ 0.10% to 0.25% carbon.
- 3) medium carbon steel ⇒ 0.25% to 0.55% carbon.
- 4) High carbon steel ⇒ 0.55% to 1.4% carbon.

physical properties of mild steels ⇒

- 1) melting point ⇒ It can be melt easily and its melting point lies in the range of  $1300^{\circ}\text{C}$  and  $1400^{\circ}\text{C}$ .
- 2) Density ⇒ Density of mild steel  $7800$  to  $7900 \text{ kg m}^{-3}$ .
- 3) shape ⇒ The shape of metal may be round square, hexagonal octagonal strip sheet angle channel, round.

Tubes and square tubes etc.

4) size  $\Rightarrow$  It is the overall dimensions of a mild steel.

5) colour  $\Rightarrow$  colour is the physical property of a metal or mild steel of displaying a particular hue in the normal daylight.

6) Lustre  $\Rightarrow$  Lustre is the property of brightness of a surface of a metal.

7) specific gravity  $\Rightarrow$  The specific gravity of mild steel is 7.85 (approximately 77.407.9)

8) porosity  $\Rightarrow$  mild steel can resist any shocks or impact loads because it is not brittle material.

9) malleability  $\Rightarrow$  The mild steel can be hammered into thin sheets because it has a character plasticity.

10) creep  $\Rightarrow$  The mild steel deforms continuously and slowly under steady load.

Chemical properties of mild steel  $\Rightarrow$

1) poor atmospheric corrosive resistance.

2) mild steel has a carbon content of between 0.16% and 0.24% maximum with a relatively high melting point.

3) low priced material with properties that are suitable for most general engineering applications.

- 4.) Low carbon mild steel has good magnetic properties.
- 5.) Due to mild steels high iron content it is therefore defined as being "ferro magnetic".
- 6.) Mild steel is not suitable for through hardening.
- 7.) Mild steel can be case hardened by being heated and a chemically reactive source of carbon added. The subsequent quench cycle will harden the surface layer.
- 8.) Mild steel - including galvanised products - is recyclable.
- 9.) Mild steel does not have a high resistance to corrosion in its untreated form.
- 10.) Mild steel can be cleaned by pickling. This is a chemical surface treatment that removes strains, contaminants, rust and scale.